Human axial progenitors generate trunk neural crest cells

Thomas J. R. Frith[1], Ilaria Granata[2], Erin Stout[1], Matthew Wind[1], Oliver Thompson[1], Katrin Neumann[3], Dylan Stavish[1], Paul R. Heath[4], James O.S. Hackland[1], Konstantinos Anastassiadis[3], Mina Gouti[5], James Briscoe[6], Val Wilson[7], Mario R. Guarracino[2], Peter W. Andrews[1], Anestis Tsakiridis[1*]

[1]Centre for Stem Cell Biology, Department of Biomedical Science, The University of Sheffield, Alfred Denny Building, Western Bank, Sheffield S10 2TN United Kingdom

[2]Computational and Data Science Laboratory (CDS-LAB), High Performance Computing and Networking Institute (ICAR), National Research Council of Italy (CNR), Via Pietro Castellino, 111, Napoli, Italy

[3]Stem Cell Engineering, Biotechnology Center, TU Dresden, Tatzberg 47, 01307 Dresden, Germany

[4]Sheffield Institute for Translational Neuroscience, University of Sheffield, 385a Glossop Road, Sheffield S10 2HQ United Kingdom

[5]Max Delbrück Center for Molecular Medicine, Robert-Rössle-Strasse 10, 13125 Berlin, Germany

[6]The Francis Crick Institute, 1 Midland Road, London, NW1 1AT United Kingdom

[7]MRC Centre for Regenerative Medicine, Institute for Stem Cell Research, School of Biological Sciences, University of Edinburgh, 5 Little France Drive, Edinburgh EH16 4UU United Kingdom

*Correspondence: a.tsakiridis@sheffield.ac.uk

Abstract

The neural crest (NC) is a multipotent embryonic cell population generating distinct cell types in an axial position-dependent manner. The production of NC cells from human pluripotent stem cells (hPSCs) is a valuable approach to study human NC biology. However, the origin of human trunk NC remains undefined and therefore current in vitro differentiation strategies induce only a modest yield of trunk NC cells. Here we show that hPSC-derived axial progenitors, the posteriorly-located drivers of embryonic axis elongation, give rise to trunk NC cells and their derivatives. Moreover, we define the molecular signatures associated with the emergence of human NC cells of distinct axial identities in vitro. Collectively, our findings indicate that there are two routes toward a human post-cranial NC state: the birth of cardiac and vagal NC is facilitated by retinoic acid-induced posteriorisation of an anterior precursor whereas trunk NC arises within a pool of posterior axial progenitors.

Introduction

The neural crest (NC) is a multipotent cell population which arises in the dorsal neural plate/non-neural ectoderm border region during vertebrate embryogenesis. Studies utilising chick and amphibian embryos have indicated that different levels of BMP, WNT and FGF signals, emanating from the mesoderm/non-neural ectoderm, orchestrate NC induction and specification (1). This occurs via the action, first of neural plate border-specific transcription factors such as PAX3/7, MSX and ZIC family members, and then via definitive NC-specifiers (e.g. SOX9/10) (2). Once specified, NC cells undergo epithelial-to-mesenchymal transition (EMT), exit the neural tube, and migrate to generate various cell types. The identity of NC products correlates to their position along the anteroposterior (A-P) axis, which is in turn reflected by the expression of paralogous HOX gene groups. Cranial NC cells give rise to mesoectodermal derivatives (e.g. dermis, cartilage, bone), melanocytes, neurons and glia colonizing the head (3) and are divided into an anterior HOX-negative and a posterior HOX group(1-3)-positive domain. The latter also includes cells contributing to heart structures (termed cardiac NC) (3, 4). Vagal NC cells, which are located between somites 1-7, are

marked by the expression of HOX group(3-5) members (5-7) and generate the enteric nervous system (ENS) (8). HOX group(5-9)-positive NC cells at the trunk level (5, 9-11) produce sympathoadrenal cells, which in turn give rise to sympathetic neurons, neuroendocrine cells, and melanocytes (12).

An attractive approach for studying human NC biology and modelling NC-associated developmental disorders (neurocristopathies) involves the in vitro differentiation of human pluripotent stem cells (hPSCs) toward NC cells. Conventional protocols to obtain NC from hPSCs are conceptually based on the production of a neurectodermal intermediate, via TGFβ signalling inhibition, which is subsequently steered toward a NC fate, usually through stimulation of WNT activity combined with the appropriate BMP level (13-16). These strategies yield NC cells of an anterior cranial character lacking HOX gene expression and the generation of more posterior HOX+ NC subtypes typically relies on the addition of retinoic acid (RA) and/or further WNT signalling stimulation (17-20). However, these signals fail to efficiently induce a high number of NC cells of a HOX(5-9)+ trunk identity from an anterior cranial progenitor. Therefore, the generation of trunk NC derivatives such as sympathoadrenal cells often requires the flow cytometry-based purification of small cell populations positive for lineage-specific fluorescent reporter (18) or cell surface markers (21), a time-consuming and laborious approach.

A number of studies in chicken and mouse embryos employing both fate mapping and lineage tracing have shown the existence of a posterior NC progenitor entity, which is distinct from its more anterior counterparts and potentially co-localises with a pool of caudally-located axial progenitors (22-27) . These progenitors include a bipotent stem cell-like population that fuels embryonic axis elongation through the coordinated production of spinal cord neurectoderm and paraxial mesoderm (PXM) (28) (reviewed in (29) and (30). In both mouse and chick embryos these neuromesodermal progenitors (NMPs) are located in the node/streak border and the caudal lateral epiblast during early somitogenesis, and later in the chordoneural hinge within the tailbud (TB) (27, 31-34). No unique NMP markers have been determined to date and thus phenotypically NMPs are defined by the co-expression of

the pro-mesodermal transcription factor Brachyury (T) and neural regulator SOX2 (35-37). Furthermore, they express transcripts which are also present in the primitive streak (PS) and TB marking committed PXM and posterior neurectodermal progenitors such as *Cdx* and *Hox* gene family members, *Tbx6* and *Nkx1-2* (23, 24, 31, 38, 39). T and SOX2 have a critical role, in conjunction with CDX and HOX proteins, in regulating the balance between NMP maintenance and differentiation by integrating inputs predominantly from the WNT and FGF signalling pathways (27, 38-41). The pivotal role of these pathways has been further demonstrated by recent studies showing that their combined stimulation results in the robust induction of T+SOX2+ NMP-like cells from mouse and human PSCs (42-44).

NMPs/axial progenitors appear to be closely related to trunk NC precursors in vivo. Specifically, trunk NC production has been shown to be controlled by transcription factors which also regulate cell fate decisions in axial progenitors such as CDX proteins (45-47) and NKX1-2 (48). The close relationship between bipotent axial and posterior NC progenitors is further supported by fate mapping experiments involving the grafting of a portion of E8.5 mouse caudal lateral epiblast T+SOX2+ cells (27) and avian embryonic TB regions (22, 34) as well as lineage tracing experiments (23, 24) which have revealed the presence of cell populations exhibiting simultaneously mesodermal, neural and NC differentiation potential. Together these findings suggest that the trunk/lumbar NC is likely to originate from a subset of axial progenitors arising near the PS/TB.

Here we sought to determine whether trunk NC is also closely related to axial progenitors in the human and thus define a robust improved protocol for the production of trunk NC cells and their products from hPSCs. We show that hPSC-derived, “pre-neural” axial progenitors contain a subpopulation that displays a BMP-dependent, mixed early NC/NMP transcriptional signature and thus is likely to represent the earliest trunk NC precursors. We demonstrate that neuromesodermal-potent axial progenitor cultures are competent to generate efficiently trunk NC cells, marked by thoracic HOX gene expression. This transition to trunk NC appears to take place via the maintenance of a CDX2/posterior HOX-positive state and the progressive amplification of an NC gene regulatory network. We

also show that "caudalisation" via RA treatment of anterior NC precursors leads to the acquisition of a mixed cardiac and vagal NC identity rather than a trunk NC character and define novel markers of distinct posterior NC subtypes. Finally, we utilise our findings to establish a protocol for the in vitro generation of PHOX2B+ sympathoadrenal cells and sympathetic neurons at high efficiency from cultures of posterior axial progenitor-derived trunk NC cells without the need for FACS-sorting to select for minor precursor subpopulations. Taken together these findings provide an insight into the mechanisms underpinning the "birth" of human NC cells at different axial levels and pave the way for the modelling of trunk NC-linked diseases such as neuroblastoma.

Results

Transcriptome analysis of human axial progenitors

We and others have previously shown that combined stimulation of the WNT and FGF signalling pathways in PSCs leads to the production of a high (>80%) percentage of T+SOX2+ cells. The resulting cultures resemble embryonic posterior axial progenitors, including NMPs, both in terms of marker expression and developmental potential (38, 42-44, 49). To interrogate the transcriptome changes associated with the induction of such progenitors in a human system and identify the presence of trunk NC precursors, we carried out RNA sequencing (RNAseq) following 3-day treatment of hPSCs with recombinant FGF2 and the WNT agonist/GSK-3 inhibitor CHIR99021 (CHIR). As reported previously, most cells emerging under these conditions co-expressed T and SOX2 as well as CDX2 (**Figure 1A**). We found that the transcriptomes of hNMPs and hPSCs were markedly distinct from each other (**Figures S1A, S1B**) and dramatic global gene expression changes accompanied the acquisition of an axial progenitor character: 1911 and 1895 genes were significantly (padj<0.05; Fold Change >= 2) up- and down-regulated compared to hPSCs respectively (**Table S1**). Predictably, the top-downregulated genes were associated with undifferentiated hPSCs (e.g. NANOG, GDF3, POU5F1), anterior neurectoderm (OTX2) and lateral/ventral mesoderm (KDR). The vast majority of the top-upregulated genes were well-established

drivers of axis elongation (e.g. *TBRA*, *CDX1/2, EVX1, MSGN1, TBX6*) and WNT/FGF/NOTCH/RA signalling pathway components, known to be expressed at high levels in the late PS/TB regions in vivo (e.g. *WNT3A/5B, RSPO3, FGF4/8, FGF17, HES7*) (**Figures 1B, S1C, S1D, Table S1**). A large fraction of upregulated genes were transcriptional regulators **(Figure S1D, Table S1**) and we found that members of HOX gene clusters belonging to paralogous groups 1-9 were strongly differentially expressed between the two groups (**Figure 1C, S1E, Table S1**). The upregulation of posterior thoracic (group 5-9) HOX transcripts as well as the presence of many transcripts (23/32) marking "late" E9.5 mouse embryonic NMPs such as CYP26A1, FGF17 and WNT5A (38) suggest that day 3 WNT-FGF-treated hPSC cultures may correspond to a more developmentally advanced axial progenitor state. Overall, these data confirm our previous observations that treatment of hPSCs with WNT and FGF agonists gives rise to cultures resembling embryonic posterior axial progenitors.

A BMP-dependent neural crest signature in human axial progenitor cultures

We next sought evidence pointing to the potential links between trunk NC and human axial progenitors. The RNAseq analysis revealed that a considerable number of genes known to collectively mark the neural plate border and early NC in vivo ("NC/border" e.g. SOX9, PAX3, MSX1/2, SNAI1/2, ZIC1/3) were also significantly upregulated in axial progenitors (**Figure 2A**), a finding which was further verified using quantitative real time PCR (qPCR) (**Figure S2A**). To exclude the possibility that the presence of such markers was the result of spontaneous differentiation of NM bipotent axial progenitors and their neural derivatives we examined their co-expression with T, a marker of both NMPs and prospective PXM. Immunostaining of d3 WNT-FGF-treated hPSC cultures showed that a considerable fraction of T+ cells also expressed the early NC markers/specifiers SOX9, SNAI2 and PAX3 (**Figure 2B**). Moreover, SOX9-positive cells were found to express low or no MSGN1 or TBX6 (**Figure S2B**) suggesting that the upregulation of border/NC markers following WNT-FGF treatment of hPSCs was unlikely to reflect the presence of committed PXM cells given that

some of these genes are also expressed in the mesoderm during axis elongation. Collectively, these findings indicate that a NC/border state probably arises within multipotent posterior axial progenitors which have not committed to a neural or mesodermal fate.

A number of both in vivo and in vitro studies have pointed to an optimal level of low/intermediate BMP signalling acting as an inducer of a NC/border character in conjunction with WNT and FGF (14, 16, 48, 50-53). We therefore examined whether hPSC-derived axial progenitor cultures exhibit endogenous BMP activity. RNAseq revealed that many BMP pathway -associated transcripts (BMP2/4/6/7 and ID1/4) were significantly upregulated compared to hPSCs (**Figure 2A**). Moreover, antibody staining showed expression of phosphorylated SMAD1/5, a readout of BMP activity (**Figure 2C**). This is extinguished upon treatment with the BMP antagonist LDN193189 (LDN) (54) during the in vitro differentiation of hPSCs to day 3 axial progenitors (**Figure 2C**). Interestingly, BMP inhibition also caused a decrease in the transcript levels of most border/NC-specific transcripts with PAX3 and MSX1 being the most severely affected (**Figure 2D**). We also observed a reduction in the NMP/late PS/TB markers CDX2 and WNT3A whereas the PXM specifier TBX6 remained relatively unaffected by LDN treatment suggesting that emergence of prospective PXM is not influenced by BMP inhibition (**Figure 2D**). By contrast, SOX2 expression was markedly increased upon LDN treatment (**Figure 2D**). Taken together these data indicate a correlation between endogenous BMP activity and the acquisition of a SOX2+low border/NC identity by posterior axial progenitors while transition toward a SOX2+ high neural fate relies on BMP antagonism in vitro.

In vitro-derived axial progenitors are a source of trunk neural crest cells

We reasoned that if posterior axial progenitors with border/NC features correspond to pioneer trunk NC precursors then they should be competent to generate definitive trunk neural crest when placed in the right culture environment. We have recently reported a protocol for the efficient generation of anterior cranial NC cells from hPSCs involving the combined stimulation of WNT signalling, TGFβ signalling inhibition and moderate BMP

activity via the parallel addition of BMP4 and the BMP type 1 receptor inhibitor DMH1 (16). Culture of day 3 WNT-FGF-treated hPSCs under these NC-inducing conditions for 5-6 days gave rise to a high number (average percentage=50% of total cells) of cells co-expressing the definitive NC marker SOX10 together with HOXC9, a readout of trunk axial identity (**Figure 3A, 3B, 3C**). A large proportion of the cultures were also SOX9+HOXC9+ further confirming an trunk NC character whereas the percentage of neural cells marked by SOX1 expression remained very low throughout the course of the differentiation (**Figure 3B, S3A, S3B**). This may indicate that posterior NC progenitors do not progress through neural commitment but rather diverge from an earlier pre-neural, border-like stage reflecting previous reports which show that NC specification takes place prior to definitive neurulation (48, 55, 56). Furthermore, during the transition toward trunk neural crest, the NMP/pre-neural marker NKX1-2 was rapidly extinguished followed shortly after by T, while CDX1 transcript levels declined more slowly (**Figure S3A, S3B**). By contrast, the expression of CDX2 and SOX9 was maintained at high levels (>70% of total cells) throughout the course of differentiation of axial progenitors to trunk NC while SOX10 expression appeared only after day 7 of differentiation (Day 0 defined as the start of axial progenitor induction from hPSCs) (**Figure S3C, data not shown**). We also confirmed the NM potency of the starting axial progenitor cultures as treatment with high levels of FGF2/CHIR and RA led to the production of TBX6+ PXM and SOX1+ spinal cord, posterior neurectoderm (PNE) cells respectively (**Figure 3A, 3D**). Taken together these data suggest that hPSC-derived NM-potent axial progenitor cultures are competent to produce trunk NC at high efficiency.

Similar to popular in vitro neural induction strategies, most current NC differentiation protocols aiming to generate posterior (e.g. trunk) cell populations from hPSCs rely on the caudalisation of an anterior ectodermal precursor via treatment with RA and/or WNT agonists (15, 17-20). Therefore, we compared our axial progenitor–based approach for generating trunk NC to a conventional strategy involving the generation of anterior cranial NC (ANC) precursor cells (16) followed by RA addition in the presence of WNT and BMP signalling (**Figure 4A**). The axial identity of the resulting cells was assessed by qPCR assay

of *HOX* transcripts corresponding to different levels along the A-P axis. In line with previous findings (17, 19) RA-treated cells expressed high levels of *HOX* group 1-5 members compared to untreated NC suggesting a posterior cranial and vagal/cardiac NC character (**Figure 3E**). However, efficient induction trunk of *HOXC8* and *9* transcripts was only achieved when posterior axial progenitors were employed as the starting population for NC generation (**Figure 3E**). Furthermore, axial progenitor-derived NC cells were marked by increased expression of the trunk NC marker *HES6*, but did not express the cranial markers *OTX2*, *DMBX1* and *LHX5* although they were positive for the "late" cranial NC transcripts (*TFA2B*, *ETS1*, *SOX8*) (57) (**Figure 3F**). We thus conclude that posterior axial progenitors are the ideal starting population for efficiently generating trunk NC in vitro whereas RA treatment of anterior NC precursors predominantly produces posterior cranial and cardiac/vagal NC cells. These data also serve as evidence supporting the notion that trunk NC precursors are likely to arise within cells with axial progenitor/NMP features rather than a caudalised anterior progenitor.

Efficient A-P patterning of human neural crest cells reveals molecular signatures of distinct axial identities

To further discern the identity of posterior NC subtypes induced either via RA treatment or an axial progenitor intermediate as well as identify unique associated molecular signatures we carried out analysis of the transcriptomes of NC cells arising under these conditions as well as those of their precursors using microarrays (**Figure 4A**). We found that axial progenitor-derived NC cells (NMP-NC d9) and their precursors (NMP-NC d6) grouped together and were distinct from a cluster containing d6 anterior cranial NC (ANC) and +RA NC cells and their common d3 progenitor (ANC d3) (**Figure 4B, S4A**). Although the three final populations exhibited distinct transcriptional profiles they all expressed pan-NC genes including "early" NC/border (MSX1/2, PAX3/7) and "late" NC (SOX10, SNAI1/2) transcripts (**Figure 4C, S4B, S4C, Table S2**). In line with our previous observations (**Figure 3C**), ANC cells failed to express any HOX transcripts, RA treatment induced anterior HOX genes and

only WNT-FGF-treated hPSCs gave rise to NC cells positive for thoracic HOX group (5-9) members (**Figure 4D**) reflecting an anterior cranial, posterior cranial/cardiac/vagal and trunk NC fate respectively. The axial identity of the resulting posterior NC subtypes was further confirmed by the observation that some of the most-upregulated transcripts in +RA cells were established posterior cranial (e.g. ALX1/3 (58)), cardiac (e.g. *FOXC1* and 2 (59); *PDGFRa* (60); *TBX2/3* (61)) and vagal/enteric NC markers (*PHOX2A* (62); *KITLG* (63); *ARPC1B* (64) (**Figure 4E)**. In contrast, known trunk NC, sympathoadrenal and sympathetic/sensory neuron regulators such as CDX2 (47), *INSM1* (65), *ISL1* (66) and *NEUROG1 (67)* were induced only in NC cells derived from axial progenitors (**Figure 4F, Table S2**). We also identified *ASLX3*, the human homologue of the Drosophila polycomb protein *asx* (68) which has been recently linked to the developmental syndrome Bainbridge-Ropers (69) as a novel trunk NC marker (**Figure 4F, Table S2)**. Transcription factors specifically induced in anterior cranial NC cells included the forkhead gene *FOXS1* which has been shown to be expressed in mouse NC derivatives (70) and *TCF7L2*, a WNT signalling effector which has been reported to harbour a NC-associated enhancer (71) (**Tables S2, S3**). Collectively these data support the idea that a mixed posterior cranial/vagal/cardiac NC character arises upon treatment of anterior NC precursors with RA whereas a *bona fide* trunk NC identity can be achieved only via an axial progenitor intermediate.

One of the most over-represented gene categories in all three axial NC subtypes were transcription factors and a common NC-specific transcription factor module was found to be expressed regardless of axial character (**Figure S4B, Table S3, Table S4**). This included well-established border/NC regulators such as *PAX3/7, MSX2, SOX9/10, TFAP2A-C* and *SNAI1/2* (**Figure S4C, Tables S3, S4**). However, the expression levels of many of these transcription factors varied between the three groups (**Figure S4C**). The highest levels of HES6, FOXD3 and MSX1/2 were found in axial progenitor-derived trunk NC cells whereas high PAX7 and SNAI1/ SOX9 expression was more prevalent in the anterior cranial and RA-treated samples respectively (**Figure S4C**). Comparison of the day 6 trunk and d3 ANC

precursor transcriptomes also revealed that expression of LHX5 and DMBX1 marks an anterior NC state whereas HES6 is associated exclusively with a trunk fate (**Figure S4D**) indicating that diversification of axial identity in NC cells starts at an early time point via the action of distinct molecular players.

Distinct routes to posterior neural crest fates

To identify candidate genes mediating the gradual lineage restriction of trunk NC precursors present in axial progenitor cultures we compared the transcriptomes of d6 trunk NC precursors and day 3 WNT-FGF-treated hPSCs (="NMPs"). We found that dramatic global gene expression changes take place during the axial progenitor-trunk NC transition (**Figure 4G, S4E**). Some of the most upregulated transcripts were the NC-specific TFAP2A/B, ETS1, SOX5 and SOX10 together with the established trunk NC specifier CDX2, the novel trunk NC marker ASLX3, the nuclear receptors NR2F1/2 and thoracic HOX genes (HOXB7, B9) (**Figure 4G, Table S4**). In contrast, signature axial progenitor transcription factors such as *T*, *MIXL1*, *NKX1-2*, anterior HOX genes (*HOXA1/B1*) and some WNT signalling components (*WNT8A/5B*) were significantly downregulated (**Figure 4G, Table S4**). Thus differentiation of trunk NC precursors appears to involve the transition from an axial progenitor-associated gene regulatory network to a NC-specifying one that incorporates factors which potentially act as general determinants of posterior cell fate (*CDX2, HOXB9*).

We also examined transcriptome changes during the transition from an anterior NC precursor state (ANC d3) to RA-posteriorised vagal/cardiac NC cells (+RA d6). The most-highly induced transcripts in posterior cranial/cardiac/vagal NC cells included the RA receptors beta and gamma (*RARb/g*) which have been involved in hindbrain and neural crest patterning (72) and the T-box transcription factor *TBX2*, a marker of cardiac NC and in vitro derived vagal/enteric NC progenitors (19) (**Table S4**). Other upregulated transcripts included the planar cell polarity (PCP) component *PRICKLE1*, a regulator of cardiac NC cell function (73) and the TGFβ signalling-associated gene *TGFBI* (**Table S4**). Anterior NC d3 precursor specific –transcripts included the border markers *PAX7* and *ZIC3* as well as the early cranial

NC transcription factors *OTX2* and *LHX5* (57) (**Table S4**). These results indicate that, in contrast to trunk NC cells, posterior cranial/ cardiac/vagal NC cells arise from an anterior neural plate border precursor through posteriorisation under the influence of RA and possibly the non-canonical WNT and TGFβ pathways.

Efficient in vitro generation of sympathoadrenal cells from axial progenitors

We next sought to determine whether trunk NC cells derived from axial progenitors are the optimal source of sympathoadrenal (SA) progenitors and their derivatives. The BMP and sonic hedgehog (SHH) signalling pathways have been shown to be critical for the specification of these lineages from NC cells (74, 75). Therefore we cultured d8 trunk NC cells generated from axial progenitors carrying a GFP reporter within the SA/sympathetic neuron regulator PHOX2B locus (18, 76), in the presence of BMP and sonic hedgehog (SHH) signalling agonists (**Figure 5A**). GFP expression was assayed after 4 days of culture of trunk NC cells in BMP4 and SHH agonists (i.e. day 12 of differentiation) (**Figure 5B**). FACS analysis revealed that the majority of cells were PHOX2B expressing (average percentage from four independent experiments=73.5%, s.d.= 6.344) (**Figure 5B**) and a large proportion of them were also positive for the early SA progenitor marker ASCL1 (77) indicating that they had acquired a symphathoadrenal identity (**Figure S5A**). Further maturation of the resulting SA progenitors in the presence of neurotrophic factors (BDNF, GDNF and NGF) for a further 6-8 days resulted in the induction of a high yield of sympathetic neurons/progenitors co-expressing PHOX2B together with the sympathetic neuron regulator GATA3 (78) (average of 40% of total cells), ASCL1 (63%) and the SA differentiation regulator *ISL1* (64%) (**Figure 5C, 5D**). A high proportion of the resulting cells also expressed the dopamine production-associated enzyme/sympathetic neuron marker tyrosine hydroxylase (TH) (79) (**Figure 5D**). Furthermore, the cultures widely expressed the peripheral nervous system marker PERIPHERIN (PRPH) (80) together with the trunk axial marker HOXC9 (**Figure S5B**). We also detected dramatic induction of *GATA3*, *ASCL1*, *TH* and *PHOX2B* transcripts (between 1000 and 1,000,000-fold) as well as other SA lineage

markers such as *GATA2, DBH* (dopamine-β-hydroxylase) and to a lesser extent *PHOX2A* using qPCR (**Figure 5E**). Together, these results suggest that the optimal route toward the efficient production of sympathoadrenal cells and sympathetic neurons from hPSCs relies on the induction of posterior axial progenitors.

Discussion

Despite progress in the optimisation of current NC differentiation protocols the in vitro generation of trunk NC cells from hPSCs remains challenging and requires FACS-sorting of selected progenitor subpopulations, a time-consuming and laborious process also associated with increased cell death. This bottleneck prevents the dissection of the mechanisms directing human NC emergence at different axial levels as well as the efficient isolation of cell types for modelling trunk NC-specific neurocristopathies such as neuroblastoma. Previous work in amniote embryos suggested that posterior (trunk/lumbosacral) NC cells arise independently from their anterior counterparts, within a pool of axial progenitors localised near the primitive streak and the tailbud during axis elongation (22, 25-28). Here we utilised these findings and exploited our ability to induce T+ NM-potent axial progenitors from hPSCs in order to use them as the optimal starting point for the efficient in vitro derivation of trunk NC (~50% HOXC9+SOX10+), SA progenitors (~70% PHOX2B-GFP+) and sympathetic neurons without the use of FACS sorting. This strategy represents a considerable improvement over current approaches, which typically yield 5-10% PHOX2B-GFP+ cells (18) and is in line with a recent study reporting the successful production of chromaffin-like cells through the use of an NC-induction protocol which transiently produces T+SOX2+ cells (20, 21).

We show that, similar to neural cells a HOX-positive posterior identity is acquired by human NC cells via two distinct routes: posterior cranial/vagal/cardiac HOX(1-5)+ NC cells emerge through the RA/WNT-induced posteriorisation of a default anterior precursor, reflecting Nieuwkoop's "activation-transformation" model, whereas HOX(5-9)+ trunk NC cells arise from a separate WNT/FGF-induced posterior axial progenitor exhibiting caudal lateral

365 epiblast/NMP features mixed with a BMP-dependent neural plate border/neural crest
366 identity (**Fig. 6**). This finding offers an explanation for the failure of current RA
367 posteriorisation-based in vitro differentiation protocols (17, 19) to yield high numbers of
368 HOX9+ trunk NC cells and should serve as the conceptual basis for the design of
369 experiments aiming to generate NC cells of a defined A-P character from hPSCs.

370 Our data indicate that a subpopulation of in vitro derived human axial progenitors
371 acquires border/early NC characteristics in response to the WNT and FGF signals present in
372 the differentiation culture media, and under the influence of autocrine BMP signalling. This is
373 in line with bulk and single cell transcriptome data showing that mouse embryonic axial
374 progenitors/NMPs express border and early NC markers (38, 41). Furthermore, our data
375 reflect findings in the chick embryo showing that an “unstable”, pre-neural plate border
376 domain, potentially defined by the co-localisation of pre-neural (*Nkx1-2)* (81) and border
377 markers such as *Pax3* (82) and *Msx1,* arises in the avian embryonic caudal lateral epibllast
378 in response to autocrine BMP, FGF (51) and possibly WNT signalling (83). We also found
379 that CDX2 expression is maintained at high levels during the generation of trunk NC
380 indicating that this transcription factor might be critical in inducing an NC character in axial
381 progenitors. CDX2 has been shown, together with β-catenin, to bind and activate neural
382 plate border/early NC specifiers such as MSX1 and ZIC1 (47, 84) and, intriguingly, ChiP-Seq
383 data from in vitro-derived mouse NMPs have revealed that many border/NC genes are direct
384 targets of CDX2 often jointly with T (e.g. PAX3, SOX9, ZIC3) (39). Collectively these findings
385 raise the possibility that β-catenin and CDX2, in conjunction with FGF/BMP signalling, may
386 be critical for the establishment of a border/NC identity in T+ axial progenitors and further
387 work is required to test this hypothesis.

388 We show that BMP/WNT treatment of human axial progenitors promotes the
389 induction of a definitive trunk NC state. This transition appears to coincide with the
390 progressive extinction of key axial progenitor genes and their replacement by a battery of
391 NC-specific transcription factors such as TFAP2B, SOX10, NR2F2 and NR2F1 while the
392 levels of some “common” axial progenitor-NC markers (e.g. SOX9, PAX3, TFAP2A and

393 SNAI2) remain high (**Figure 4, S3, Table S4**). TFAP2A has been previously reported to act
394 as a master NC transcription factor whose binding on key enhancers, together with
395 NR2F1/2, appears to initiate transcription of NC-specific genes (71). This finding raises the
396 possibility that these transcription factors are the molecular drivers of the transition from an
397 early posterior axial progenitor state to a lineage-restricted trunk NC fate in response to
398 BMP/WNT. How is a trunk axial character specified? Our transcriptome analysis data
399 suggest that a generic trunk identity is first installed during the emergence of multipotent
400 CDX2+trunk HOX+ axial progenitors under the influence of WNT-FGF activity and then
401 "converted" into posterior NC through the progressive accumulation of neural plate
402 border/definitive NC markers within BMP-responsive cells. The posterior character of these
403 incipient trunk NC precursors and their progeny is likely to be maintained via continuous
404 CDX2 expression and further potentiation of trunk HOX activities as indicated by the
405 expression profiles of these genes in both d6 precursor and d9 trunk NC cells (**Figure 4, S4,**
406 **Tables S2-4**) and their reported roles in trunk NC specification. However, other trunk NC-
407 specific regulators may also be involved in this process and loss-/ gain-of-function
408 approaches are required to dissect their exact involvement in programming trunk identity.
409

410 **Acknowledgements**

411 We would like to thank Gabsang Lee and Lorenz Studer for providing the PHOX2B-GFP and
412 SOX10-GFP reporter hPSC lines respectively. T.F. was supported by a University of
413 Sheffield, Biomedical Science Departmental PhD studentship. A.T. is supported by funding
414 from the BBSRC (New Investigator Research Grant, BB/P000444/1), the Royal Society
415 (RG160249) and the Children's Cancer and Leukaemia Group/Little Princess Trust (CCLGA
416 2016 01). K.A. and P.W.A. are supported by the EU 7th Framework project PluriMes. M.G.
417 was supported by a BBSRC grant (BB/J015539/1). J.B. is supported by the Francis Crick
418 Institute which receives its funding from Cancer Research UK (FC001051), the UK Medical
419 Research Council (FC001051), and the Wellcome Trust (FC001051). V.W. is supported by
420 an MRC Programme Grant (Mr/K011200/1). We would like to thank Vicki Metzis, Celine

Souilhol, Ben Steventon, Matt Towers and Heiko Wurdak for critical reading of the manuscript.

Author Contributions

Conceptualization: TJRF, AT

Data Curation: IG

Formal Analysis: TJRF, IG, AT

Resources: JB, MG, TJRF, KN, KA, AT

Funding Acquisition: AT, PWA, VW, JB, MG, KA, MRG

Investigation: TJRF, IG, MW, ES, OT, JOSH, DS, PH, MG, AT

Project Administration: AT

Supervision: AT, PWA

Writing – Original Draft Preparation: AT with input from TJRF, IG

Writing – Review & Editing: All co-authors

Competing interests

The authors have no competing interests to declare

Figure legends

Figure 1. Transcriptome analysis of in vitro-derived human axial progenitors

(A) Immunofluorescence analysis of expression of indicated markers in day 3 hPSC-derived axial progenitors. Magnified regions corresponding to the insets are also shown. (B) Heatmap showing the expression values of selected markers in three independent axial progenitor and hPSC sample replicates. The expression values (FPKM) were scaled to the row mean. The color key relates the heat map colors to the standard score (z-score). (C) Induction of all significantly upregulated HOX transcripts in axial progenitors relative to hPSCs. Paralogous HOX groups corresponding to different axial levels such as cervical

(groups 1-4), brachial/thoracic (5-9) and lumbosacral (10-13) are indicated. See also Figure S1 and Table S1.

Figure 2. hNMP cultures exhibit a BMP-dependent neural crest/border signature

(A) Log-fold induction of representative neural crest/neural plate border and BMP-associated transcripts in axial progenitors compared to hESCs. (B) Immunofluorescence analysis of expression of indicated markers in axial progenitos. Magnified regions corresponding to the insets are also shown. (C) Immunofluorescence analysis of expression of phosphorylated SMAD1/5 (p-SMAD) in the presence and absence of the BMP inhibitor LDN193189 (LDN). (D) qPCR expression analysis of indicated markers in axial progenitors in the presence (+) or absence (-) of LDN. Error bars=S.D. (n=2). In all cases nuclei were counterstained with DAPI. PXM, paraxial mesoderm; NC, neural crest. See also Figure S2.

Figure 3. In vitro derived axial progenitors generate trunk neural crest efficiently

(A) Diagram depicting the culture conditions employed to direct trunk NC, posterior neurectoderm (PNE) and paraxial mesoderm (PXM) differentiation from hPSC-derived axial progenitors. (B) Immunofluorescence analysis of the expression of indicated NC (SOX10, SOX9) and neural (SOX1) and the thoracic/trunk marker HOXC9 in trunk NC (TNC) cells derived from axial progenitors after 8 days of differentiation. Magnified regions corresponding to the insets are also shown. Note that the HOXC9/SOX10 and SOX10/SOX1 image sets correspond to the same cells. (C) Quantitation of cells marked by different combinations of HOXC9 and SOX10 expression in day 8 trunk NC cultures derived from axial progenitors following image analysis. Six randomly selected fields (two independent experiments) were used for analysis (total number of cells scored= 5366, average number of cells/field=894, error bars=s.d.). (D) Immunofluorescence analysis of TBX6 (left) or SOX1 (right) expression in axial progenitors treated with CHIR-FGF2 (pro-PXM conditions) and RA (pro-PNE conditions) respectively. (E) qPCR expression analysis of indicated HOX genes in hPSC-derived anterior cranial (ANC), retinoic acid (RA)-treated NC (+RA), and axial progenitor-derived NC cells (NMP-NC) relative to hPSCs. Error bars=S.E.M. (n=3). (F) qPCR expression analysis of indicated NC markers in +RA and axial progenitor-derived NC

cells relative to untreated anterior cranial NC cells. Error bars=S.E.M. (n=3). See also Figure S3.

Figure 4. Transcriptome analysis of in vitro derived neural crest cells corresponding to distinct axial levels

(A) Diagrams showing the culture conditions employed for generating NC cells of distinct axial identities using hPSCs. Asterisks indicate the timepoints used for sample harvesting and transcriptome analysis. D, day of differentiation. ANC, Anterior neural crest. (B) Principal component analysis depicting variance between different samples used for microarray analysis (timepoints shown in A). (C) Venn diagram showing the overlap between all significantly upregulated (≥2-fold relative to undifferentiated hESCs, FDR ≤ 0.05) in each indicated NC group. (D) Log fold induction of HOX genes in indicated NC populations relative to hPSCs. (E) Log fold induction of representative significantly upregulated (≥2-fold relative to undifferentiated hPSCs, FDR ≤ 0.05) transcripts marking day 6 RA-treated NC cells. (F) Log fold induction of representative significantly upregulated (≥2-fold relative to undifferentiated hPSCs, FDR ≤ 0.05) transcripts marking day 9 axial progenitor-derived NC cells. (G) Log fold changes in the expression of the most-upregulated and most-downregulated transcripts in day 6 axial progenitor-derived NC precursors compared to d3 hPSC-derived axial progenitors. See also Figure S4, Tables S2, S3, and S4.

Figure 5. Axial progenitor-derived trunk neural crest is an optimal source of sympathoadrenal cells

(A) Diagram depicting the culture conditions employed to direct axial progenitors (“NMPs”) toward trunk NC and subsequently sympathoadrenal progenitors (SAP) and sympathetic neurons. (B) FACS analysis of PHOX2B-GFP expression in SAP cells derived from axial progenitors as shown in A. Below: Immunofluorescence analysis of PHOX2B-GFP and PHOX2B protein expression following antibody staining. (C) Quantitation of d18 differentiated cells positive for the indicated markers in relation to PHOX2B-GFP expression following antibody staining. In each case four randomly selected representative fields were used to obtain the average number of cells/marker. Total numbers of cells scored: GATA3

(N=3003), ASCL1 (N=2575), ISL1 (N=2963). (D) Immunofluorescence analysis of PHOX2B-GFP together with the indicated markers in day 18 differentiated SAP/sympathetic neurons derived from axial progenitors as shown in A. (E) qPCR expression analysis of indicated SAP/sympathetic neuron markers in d12 and d18 cultures. Error bars=S.E.M. (n=3). See also Figure S5.

Figure 6. A-P patterning of in vitro derived human NC cells

Diagrammatic model summarising our findings on the in vitro generation of NC subtypes of distinct A-P identity from hPSCs. Examples of unique genes that were found to mark each NC population exclusively are shown in red.

Supplemental Figure Legends

Figure S1

(A) Dendrogram showing the clustering of the individual axial progenitor (NMP) and hESC sample replicates based on RNAseq expression data. (B) Principal Component Analysis (PCA) plot indicates a good separation, in terms of gene expression, between the two conditions and a good replication among samples. ((C) Volcano plot reporting pvalue (y axis) as a function of log2 fold change (x axis) between the axial progenitor and hPSC groups. The red dots depict significant genes (pvalue<=0.05). Top differentially expressed transcriptional regulators of axis elongation and WNT/FGF/NOTCH/RA signalling pathway components are shown. (D) Top gene ontology groups significantly enriched in axial progenitors vs hPSCs. (E) Hierarchical clustering heatmap showing the expression values of HOX genes in axial progenitor and hPSC sample replicates. The expression values (FPKM) were scaled to the row mean. The color key relates the heat map colors to the standard score (z-score).

Figure S2.

(A) qPCR expression analysis of indicated NC/border and pluripotency markers in axial progenitors vs hPSCs. Error bars=S.E.M. (n=3). (B) Immunofluorescence analysis of SOX9

532 expression together with MSGN1-VENUS (top) and TBX6 (bottom) in axial progenitors
533 derived from a MSGN1-VENUS or wild type hPSCs respectively.

534 **Figure S3**

535 (A) Immunofluorescence analysis of indicated markers one (day 4 of differentiation) or two
536 (day 5 of differentiation) days after re-plating axial progenitors into NC inducing conditions.
537 (B) qPCR expression analysis of indicated axial progenitor (NMP) and neural markers during
538 differentiation toward TNC. Error bars=s.e.m. (n=3) (C) Immunofluorescence analysis of
539 indicated NC markers one (day 4 of differentiation) or two (day 5 of differentiation) days after
540 re-plating axial progenitors into NC inducing conditions.

541 **Figure S4**

542 (A) Heatmap showing Pearson's signal correlation between indicated samples. (B) Venn
543 diagram showing the overlap between transcription factors (TFs) enriched (≥2-fold relative to
544 undifferentiated hPSCs, FDR ≤ 0.05) in each indicated NC group of distinct axial identity.
545 The detailed list of all TFs can be found in Table S3. (C) Heatmap showing relative
546 expression of representative NC markers in NC populations of distinct axial identity and
547 hPSCs. (D) Heatmap showing relative expression of representative NC markers in trunk and
548 anterior cranial NC precursors and hPSCs. (E) Volcano plot depicting upregulated (red) and
549 downregulated (green) genes in d6 trunk NC precursors (NMP-NC) vs axial progenitors
550 (=NMPs).

551 **Figure S5**

552 (A) Immunofluorescence analysis of PHOX2B-GFP and ASCL1 expression in d12 SAP cells
553 derived from axial progenitors as shown in Fig. 5A. (B) Immunofluorescence analysis of
554 PRPH and HOXC9 expression in sympathetic neurons derived from axial progenitors as
555 shown in Fig. 5A.

556

557 **Table S1.** Significantly up- and downregulated transcripts, GO enrichment and TF
558 signatures from RNAseq analysis

559 **Table S2.** List of genes upregulated in different NC populations and GO enrichment analysis

560 **Table S3.** List of transcription factors shared between different NC populations

561 **Table S4.** List of all genes up- and down-regulated in indicated NC populations and their
562 progenitors.

563 **Table S5.** List of primers

564

565 **METHODS**

566 **Cell culture and differentiation**

567 We employed the following hPSC lines: a Shef4-derived Sox2-GFP reporter hESC line (44),
568 the H9-derived SOX10-GFP (15) and PHOX2B-GFP (18) reporter hESC lines, the MSGN1-
569 VENUS reporter hiPSC line, and the unmodified Mastershef7 hESC line (44) and an iPSC
570 line (MIFF-1) derived from a healthy individual (85). The MSGN1-Venus reporter line was
571 generated by Transposon mediated BAC transgenesis using protocols described by (86). In
572 brief, a human BAC (RP11-12L16) with piggyBac transposon repeats flanking the bacterial
573 backbone and with Venus inserted directly after the initiating methionine of MSGN1 was
574 transfected together with a piggyBac Transposase into NCRM1 iPSCs. Cells were cultured
575 in feeder-free conditions in either Essential 8 (Thermo Fisher) or mTeSR1 (Stem Cell
576 Technologies) medium on laminin 521 (Biolamina) or vitronectin (Thermo Fisher). All
577 differentiation experiments were carried out in at least three different hPSC line. For
578 NMP/axial progenitor differentiation hPSCs were dissociated using PBS/EDTA and plated at
579 a density of 55,000 cells/cm^2 (density optimised for 12-well plates) on fibronectin (Sigma) or
580 vitronectin (Thermo Fisher)-coated wells, directly into NMP-inducing medium containing
581 CHIR99021 (Tocris), FGF2 (20 ng/ml, Peprotech) and ROCK inhibitor Y-27632 for the first
582 only day (10 µM, Tocris). We observed some variation in terms of induction of T+SOX2+
583 NMPs both between hPSC lines and also batches of CHIR99021 and thus the concentration
584 of the latter was varied between 3-4 µM. BMP inhibition was carried out using LDN193189
585 (Tocris) at 100 nM. For trunk NC differentiation day 3 hPSC-derived axial progenitors were
586 dissociated using accutase and re-plated at a density 30,000 cells /cm^2 on Geltrex (Thermo
587 Fisher)-coated plates directly into NC-inducing medium containing DMEM/F12 (Sigma), 1x

588 N2 supplement (Thermo Fisher), 1x Non-essential amino acids (Thermo Fisher) and 1x
589 Glutamax (Thermo Fisher), the TGFb/Nodal inhibitor SB431542 (2 µM, Tocris), CHIR99021
590 (1 µM, Tocris), DMH1 (1 µM, Tocris), BMP4 (15 ng/ml, Thermo Fisher) and Y-27632 (10
591 µM, Tocris). The medium was replaced at days 5 and 7 of differentiation but without the
592 ROCK inhibitor and trunk NC cells were analysed either at day 8 or 9. For cranial neural
593 crest differentiation hPSCs were dissociated using accutase and plated under the same NC-
594 inducing conditions as described above for 5-6 days. For posterior cranial/vagal/cardiac NC
595 generation d4 differentiated anterior NC progenitors induced as described above were
596 treated with retinoic acid (1 µM, Tocris) in the presence of the NC-inducing medium till day 6
597 of differentiation. For sympathoadrenal progenitor (SAP) differentiation d8 trunk NC cells
598 were re-suspended at a density of 200-300,000 cells /cm^2 on Geltrex (Thermo Fisher)-
599 coated plates directly into medium containing BrainPhys neuronal medium (Stem Cell
600 Technologies), 1x B27 supplement (Thermo Fisher), 1x N2 supplement (Thermo Fisher), 1x
601 Non-essential amino acids (Thermo Fisher) and 1x Glutamax (Thermo Fisher), BMP4 (50
602 ng/ml, Thermo Fisher), recombinant SHH (C25II) (50 ng/ml, R&D) and purmorphamine
603 (1.25-1.5 µM, Millipore) and cultured for 4 days (d12 of differentiation). For further
604 sympathetic neuron differentiation d12 SAP cells were switched into a medium containing
605 BrainPhys neuronal medium (Stem Cell Technologies), 1x B27 supplement (Thermo Fisher),
606 1x N2 supplement (Thermo Fisher), 1x Non-essential amino acids (Thermo Fisher) and 1x
607 Glutamax (Thermo Fisher), ascorbic acid (200 µM, Sigma) , NGF (10 ng/ml, Peprotech),
608 BDNF (10 ng/ml, Peprotech) and GDNF (10 ng/ml, Peprotech) and cultured for a further 6-8
609 days. For paraxial mesoderm differentiation d3 axial progenitor cultures were treated with
610 accutase and replated at a density of 45,000/cm^2 on 12-well Geltrex-coated plates in N2B27
611 containing FGF2 (40 ng/ml, Peprotech) and CHIR99021 (8 µM, Tocris) for two days. For
612 neural differentiation d3 axial progenitor cultures were treated with accutase and replated at
613 a density of 45,000/cm^2 on 12-well Geltrex-coated plates in N2B27 containing 100 nM
614 retinoic acid (Tocris) for 2-3 days.

615 **RNA sequencing**

616 *Sample preparation*

617 For RNA sequencing we employed hESCs or axial progenitors following culture on
618 fibronectin in FGF2 (20 ng/ml) and CHIR99021 (3 μM). Total RNA from NMPs and hESCs
619 was harvested using the RNeasy kit (Qiagen) according to the manufacturer's instructions.

620 *Library preparation/sequencing*

621 Total RNA was processed according to the TruSeq protocol (Illumina). Three separate RNA
622 libraries (biological replicates) were barcoded and prepared for hPSCs and D3 axial
623 progenitors. Library size, purity and concentration were determined using the Agilent
624 Technologies 2100 Bioanalyzer. For sequencing, four samples were loaded per lane on an
625 Illumina Genome Analyzer Hiseq2500.

626 *RNAseq quality control and mapping*

627 The quality of raw reads in fastq format was analyzed by FastQC
628 (http://www.bioinformatics.babraham.ac.uk/projects/fastqc). Adapter contamination and poor
629 quality ends were removed using Trim Galore v. 0.4.0 (Babraham Bioinformatics - Trim
630 Galore! Available at: http://www.bioinformatics.babraham.ac.uk/projects/trim_galore/).
631 Single-end clean reads were aligned to the human reference genome (hg38 assembly) using
632 Tophat2 v2.0.13 (87).

633 *RNA seq data analysis*

634 Read alignments were sorted with SAMtools v1.1 before being counted to genomic features
635 by HTSeq version 0.6.0 (88). The average overall read alignment rate across all samples
636 was 94.3%. Differential gene expression was performed using DESeq2 version 1.16.1 (89).
637 in R version 3.3.3. Genes were considered significantly differentially expressed (DE) with a
638 Benjamini-Hochberg adjusted pvalue <=0.05 and a log2FoldChange> |1|. Gene Ontology
639 (GO) biological processes (BP) enrichment analysis was carried out for DE genes using the
640 DAVID gene ontology functional annotation tool (https://david.ncifcrf.gov/)
641 (90, 91) with default parameters. We considered as significant terms having a FDR adjusted
642 pvalue <= 0.05, which is derived from a modified Fisher's exact test.

643

644 **Microarrays**

645 *Sample preparation and processing*

646 Samples were prepared according to the Affymetrix WT Plus protocol for Gene Chip ®
647 Whole Transcript Expression Arrays. Briefly 200ng of high quality total RNA, (RNA integrity
648 number (RIN) greater than 9), was converted to double stranded cDNA with the introduction
649 of a T7 polymerase binding site. This allowed the synthesis of an antisense RNA molecule
650 against which a sense DNA strand was prepared. The RNA strand was digested and the
651 resulting single stranded DNA fragmented and biotin labelled. Along with appropriate
652 controls the labelled fragmented DNA was hybridised to Affymetrix Clariom D arrays
653 overnight using the Affymetrix 640 hybridisation oven; 16 hours with rotation at 60 rpm at
654 45^0C. The arrays were washed and stained according to standard protocols which allowed
655 the introduction of streptavidin-phycoerythrin in order to generate a fluorescent signal from
656 the hybridised biotinylated fragments. The washed and stained arrays were scanned using
657 the Affymetrix 3000 7G scanner with autoloader. The generated CEL files were taken
658 forward for analysis.

659 *Data analysis*

660 Data were analysed using the Affymetrix Transcriptome Analysis Console 4.0 software.
661 Analysis of Expression (Gene+Exon) was used to generate lists of all differentially
662 expressed genes showing >2; <-2 fold Log Change and P<0.05. For the distance matrix
663 (**Figure S4A**), Exploratory Grouping analysis was used. Log_2 normalised intensity data
664 values were mapped in R using the package 'pheatmap' with correlation clustering by gene.
665 Gene ontology analysis was carried out using the ToppGene suite
666 (https://toppgene.cchmc.org/enrichment.jsp) (92). Area proportional 3-Venn diagrams were
667 drawn using the eulerApe software (93).

668 **Quantitative real time PCR**

669 Total RNA from different samples was harvested using the RNeasy kit (Qiagen) according to
670 the manufacturer's instructions and digested with DNase I (Qiagen) to remove genomic
671 DNA. First strand cDNA synthesis was performed using the Superscript III system (Thermo

672 Fisher) using random primers. Quantitative real time PCR was carried out using the Applied
673 Biosystems QuantStudio™ 12K Flex thermocycler together with the Roche UPL system.
674 Primer sequences are shown in Table S5.

675 **Flow cytometry**

676 Cells were lifted into a single cell suspension using Accutase (as previously described) and
677 resuspended in FACS buffer (DMEM with 10% v/v FCS) to neutralise Accutase before
678 centrifugation at 1100rpm/4min. Cells were then resuspended in FACs buffer at 1x106
679 cells/ml and 100,000 cells were placed in FACs tubes (Falcon 352053). A GFP baseline was
680 set using unmodified wild type control cells.

681 **Immunofluorescence**

682 Cells were fixed for 10 minutes at 4°C in 4% paraformaldehyde (PFA) in phosphate buffer
683 saline (PBS), then washed in PBST (PBS with 0.1% Triton X-100) and treated with 0.5 M
684 glycine/PBST to quench the PFA. Blocking was then carried for 1-3 h in PBST supplemented
685 with 3% donkey serum/1% BSA at room temperature or overnight at 4^0C. Primary and
686 secondary antibodies were diluted in PBST containing in PBST supplemented with 3%
687 donkey serum/1% BSA. Cells were incubated with primary antibodies overnight at 4°C and
688 with secondary antibodies at room temperature for 2 h in the dark. Cell nuclei were
689 counterstained using Hoechst 33342 (1:1000, Thermo Fisher) and fluorescent images were
690 taken using the InCell Analyser 2500 system (GE Healthcare). We used the following
691 antibodies: anti-T (1:200; AF2085, R&D), anti-SOX2 (1:200; ab92494, Abcam), anti-SOX9
692 (1:200; 82630, CST), anti-SNAI2 (1:400; C19G7, CST), anti-PAX3 (1:50; DSHB), anti-
693 phosphoSMAD1/5/9 (1:100; D5B10, CST), anti-SOX10 (1:200; D5V9L, CST), anti-SOX1
694 (1:100; AF3369, R&D), anti-TBX6 (1:50, AF4744, R7D) anti-TH (1:1000; T1299, SIGMA),
695 HOXC9 (1:50; ab50839, Abcam) anti-PRPH (1:100; AB1530, Millipore), anti-CDX2 (1:200;
696 ab76541, Abcam), anti-ASCL1 (1:100; 556604, BD Pharmigen), anti-GATA3 (1:100; sc-269,
697 Santa Cruz), anti-GFP (1:1000; ab13970, Abcam), anti-ISL1 (1:100, DSHB), anti-PHOX2B
698 (1:100; sc-376997, Santa Cruz). Images were processed using Photoshop and Fiji. Nuclear

699 segmentation followed by single cell fluorescence quantification was performed as described
700 previously using Fiji and the MultiCell3D application as described previously (35, 94).

701 **Data availability**

702 The microarray and RNAseq data have been deposited to GEO (GSE109267 and
703 GSE110608).

704

705

706

707 **REFERENCES**

708 1. Stuhlmiller TJ, Garcia-Castro MI. Current perspectives of the signaling pathways directing
709 neural crest induction. Cell Mol Life Sci. 2012;69(22):3715-37.
710 2. Simoes-Costa M, Bronner ME. Establishing neural crest identity: a gene regulatory recipe.
711 Development. 2015;142(2):242-57.
712 3. Le Douarin NM, Creuzet S, Couly G, Dupin E. Neural crest cell plasticity and its limits.
713 Development. 2004;131(19):4637-50.
714 4. Kirby ML, Gale TF, Stewart DE. Neural crest cells contribute to normal aorticopulmonary
715 septation. Science. 1983;220(4601):1059-61.
716 5. Kam MK, Lui VC. Roles of Hoxb5 in the development of vagal and trunk neural crest cells.
717 Dev Growth Differ. 2015;57(2):158-68.
718 6. Fu M, Lui VC, Sham MH, Cheung AN, Tam PK. HOXB5 expression is spatially and temporarily
719 regulated in human embryonic gut during neural crest cell colonization and differentiation of enteric
720 neuroblasts. Dev Dyn. 2003;228(1):1-10.
721 7. Chan KK, Chen YS, Yau TO, Fu M, Lui VC, Tam PK, et al. Hoxb3 vagal neural crest-specific
722 enhancer element for controlling enteric nervous system development. Dev Dyn. 2005;233(2):473-
723 83.
724 8. Le Douarin NM, Teillet MA. The migration of neural crest cells to the wall of the digestive
725 tract in avian embryo. J Embryol Exp Morphol. 1973;30(1):31-48.
726 9. Nguyen MT, Zhu J, Nakamura E, Bao X, Mackem S. Tamoxifen-dependent, inducible
727 Hoxb6CreERT recombinase function in lateral plate and limb mesoderm, CNS isthmic organizer,
728 posterior trunk neural crest, hindgut, and tailbud. Dev Dyn. 2009;238(2):467-74.
729 10. Ishikawa S, Ito K. Plasticity and regulatory mechanisms of Hox gene expression in mouse
730 neural crest cells. Cell Tissue Res. 2009;337(3):381-91.
731 11. Huber L, Ferdin M, Holzmann J, Stubbusch J, Rohrer H. HoxB8 in noradrenergic specification
732 and differentiation of the autonomic nervous system. Dev Biol. 2012;363(1):219-33.
733 12. Le Douarin NM, Teillet MA. Experimental analysis of the migration and differentiation of
734 neuroblasts of the autonomic nervous system and of neurectodermal mesenchymal derivatives,
735 using a biological cell marking technique. Dev Biol. 1974;41(1):162-84.
736 13. Lee G, Kim H, Elkabetz Y, Al Shamy G, Panagiotakos G, Barberi T, et al. Isolation and directed
737 differentiation of neural crest stem cells derived from human embryonic stem cells. Nat Biotechnol.
738 2007;25(12):1468-75.

14. Menendez L, Yatskievych TA, Antin PB, Dalton S. Wnt signaling and a Smad pathway blockade direct the differentiation of human pluripotent stem cells to multipotent neural crest cells. Proc Natl Acad Sci U S A. 2011;108(48):19240-5.
15. Chambers SM, Qi Y, Mica Y, Lee G, Zhang XJ, Niu L, et al. Combined small-molecule inhibition accelerates developmental timing and converts human pluripotent stem cells into nociceptors. Nat Biotechnol. 2012;30(7):715-20.
16. Hackland JOS, Frith TJR, Thompson O, Marin Navarro A, Garcia-Castro MI, Unger C, et al. Top-Down Inhibition of BMP Signaling Enables Robust Induction of hPSCs Into Neural Crest in Fully Defined, Xeno-free Conditions. Stem Cell Reports. 2017.
17. Huang M, Miller ML, McHenry LK, Zheng T, Zhen Q, Ilkhanizadeh S, et al. Generating trunk neural crest from human pluripotent stem cells. Sci Rep. 2016;6:19727.
18. Oh Y, Cho GS, Li Z, Hong I, Zhu R, Kim MJ, et al. Functional Coupling with Cardiac Muscle Promotes Maturation of hPSC-Derived Sympathetic Neurons. Cell Stem Cell. 2016;19(1):95-106.
19. Fattahi F, Steinbeck JA, Kriks S, Tchieu J, Zimmer B, Kishinevsky S, et al. Deriving human ENS lineages for cell therapy and drug discovery in Hirschsprung disease. Nature. 2016;531(7592):105-9.
20. Denham M, Hasegawa K, Menheniott T, Rollo B, Zhang D, Hough S, et al. Multipotent caudal neural progenitors derived from human pluripotent stem cells that give rise to lineages of the central and peripheral nervous system. Stem Cells. 2015;33(6):1759-70.
21. Abu-Bonsrah KD, Zhang D, Bjorksten AR, Dottori M, Newgreen DF. Generation of Adrenal Chromaffin-like Cells from Human Pluripotent Stem Cells. Stem Cell Reports. 2017.
22. Catala M, Teillet MA, Le Douarin NM. Organization and development of the tail bud analyzed with the quail-chick chimaera system. Mech Dev. 1995;51(1):51-65.
23. Albors A, Halley P, Storey KG. Fate mapping caudal lateral epiblast reveals continuous contribution to neural and mesodermal lineages and the origin of secondary neural tube. bioRxiv. 2016.
24. Javali A, Misra A, Leonavicius K, Acharyya D, Vyas B, Sambasivan R. Co-expression of Tbx6 and Sox2 identifies a novel transient neuromesoderm progenitor cell state. Development. 2017;144(24):4522-9.
25. Schoenwolf GC, Chandler NB, Smith JL. Analysis of the origins and early fates of neural crest cells in caudal regions of avian embryos. Dev Biol. 1985;110(2):467-79.
26. Schoenwolf GC, Nichols DH. Histological and ultrastructural studies on the origin of caudal neural crest cells in mouse embryos. J Comp Neurol. 1984;222(4):496-505.
27. Wymeersch FJ, Huang Y, Blin G, Cambray N, Wilkie R, Wong FC, et al. Position-dependent plasticity of distinct progenitor types in the primitive streak. Elife. 2016;5:e10042.
28. Tzouanacou E, Wegener A, Wymeersch FJ, Wilson V, Nicolas JF. Redefining the progression of lineage segregations during mammalian embryogenesis by clonal analysis. Dev Cell. 2009;17(3):365-76.
29. Steventon B, Martinez Arias A. Evo-engineering and the cellular and molecular origins of the vertebrate spinal cord. Dev Biol. 2017.
30. Henrique D, Abranches E, Verrier L, Storey KG. Neuromesodermal progenitors and the making of the spinal cord. Development. 2015;142(17):2864-75.
31. Cambray N, Wilson V. Two distinct sources for a population of maturing axial progenitors. Development. 2007;134(15):2829-40.
32. Cambray N, Wilson V. Axial progenitors with extensive potency are localised to the mouse chordoneural hinge. Development. 2002;129(20):4855-66.
33. Brown JM, Storey KG. A region of the vertebrate neural plate in which neighbouring cells can adopt neural or epidermal fates. Curr Biol. 2000;10(14):869-72.
34. McGrew MJ, Sherman A, Lillico SG, Ellard FM, Radcliffe PA, Gilhooley HJ, et al. Localised axial progenitor cell populations in the avian tail bud are not committed to a posterior Hox identity. Development. 2008;135(13):2289-99.

35. Tsakiridis A, Huang Y, Blin G, Skylaki S, Wymeersch F, Osorno R, et al. Distinct Wnt-driven primitive streak-like populations reflect in vivo lineage precursors. Development. 2014;141(6):1209-21.
36. Olivera-Martinez I, Harada H, Halley PA, Storey KG. Loss of FGF-dependent mesoderm identity and rise of endogenous retinoid signalling determine cessation of body axis elongation. PLoS Biol. 2012;10(10):e1001415.
37. Martin BL, Kimelman D. Canonical Wnt signaling dynamically controls multiple stem cell fate decisions during vertebrate body formation. Dev Cell. 2012;22(1):223-32.
38. Gouti M, Delile J, Stamataki D, Wymeersch FJ, Huang Y, Kleinjung J, et al. A Gene Regulatory Network Balances Neural and Mesoderm Specification during Vertebrate Trunk Development. Dev Cell. 2017;41(3):243-61 e7.
39. Amin S, Neijts R, Simmini S, van Rooijen C, Tan SC, Kester L, et al. Cdx and T Brachyury Co-activate Growth Signaling in the Embryonic Axial Progenitor Niche. Cell Rep. 2016;17(12):3165-77.
40. Young T, Rowland JE, van de Ven C, Bialecka M, Novoa A, Carapuco M, et al. Cdx and Hox genes differentially regulate posterior axial growth in mammalian embryos. Dev Cell. 2009;17(4):516-26.
41. Koch F, Scholze M, Wittler L, Schifferl D, Sudheer S, Grote P, et al. Antagonistic Activities of Sox2 and Brachyury Control the Fate Choice of Neuro-Mesodermal Progenitors. Dev Cell. 2017;42(5):514-26 e7.
42. Turner DA, Hayward PC, Baillie-Johnson P, Rue P, Broome R, Faunes F, et al. Wnt/beta-catenin and FGF signalling direct the specification and maintenance of a neuromesodermal axial progenitor in ensembles of mouse embryonic stem cells. Development. 2014;141(22):4243-53.
43. Lippmann ES, Williams CE, Ruhl DA, Estevez-Silva MC, Chapman ER, Coon JJ, et al. Deterministic HOX patterning in human pluripotent stem cell-derived neuroectoderm. Stem Cell Reports. 2015;4(4):632-44.
44. Gouti M, Tsakiridis A, Wymeersch FJ, Huang Y, Kleinjung J, Wilson V, et al. In vitro generation of neuromesodermal progenitors reveals distinct roles for wnt signalling in the specification of spinal cord and paraxial mesoderm identity. PLoS Biol. 2014;12(8):e1001937.
45. Sanchez-Ferras O, Coutaud B, Djavanbakht Samani T, Tremblay I, Souchkova O, Pilon N. Caudal-related homeobox (Cdx) protein-dependent integration of canonical Wnt signaling on paired-box 3 (Pax3) neural crest enhancer. J Biol Chem. 2012;287(20):16623-35.
46. Sanchez-Ferras O, Bernas G, Laberge-Perrault E, Pilon N. Induction and dorsal restriction of Paired-box 3 (Pax3) gene expression in the caudal neuroectoderm is mediated by integration of multiple pathways on a short neural crest enhancer. Biochim Biophys Acta. 2014;1839(7):546-58.
47. Sanchez-Ferras O, Bernas G, Farnos O, Toure AM, Souchkova O, Pilon N. A direct role for murine Cdx proteins in the trunk neural crest gene regulatory network. Development. 2016;143(8):1363-74.
48. Sasai N, Kutejova E, Briscoe J. Integration of signals along orthogonal axes of the vertebrate neural tube controls progenitor competence and increases cell diversity. PLoS Biol. 2014;12(7):e1001907.
49. Tsakiridis A, Wilson V. Assessing the bipotency of in vitro-derived neuromesodermal progenitors. F1000Res. 2015;4:100.
50. Tribulo C, Aybar MJ, Nguyen VH, Mullins MC, Mayor R. Regulation of Msx genes by a Bmp gradient is essential for neural crest specification. Development. 2003;130(26):6441-52.
51. Streit A, Stern CD. Establishment and maintenance of the border of the neural plate in the chick: involvement of FGF and BMP activity. Mech Dev. 1999;82(1-2):51-66.
52. Patthey C, Edlund T, Gunhaga L. Wnt-regulated temporal control of BMP exposure directs the choice between neural plate border and epidermal fate. Development. 2009;136(1):73-83.
53. Marchant L, Linker C, Ruiz P, Guerrero N, Mayor R. The inductive properties of mesoderm suggest that the neural crest cells are specified by a BMP gradient. Dev Biol. 1998;198(2):319-29.

839 54. Cuny GD, Yu PB, Laha JK, Xing X, Liu JF, Lai CS, et al. Structure-activity relationship study of
840 bone morphogenetic protein (BMP) signaling inhibitors. Bioorg Med Chem Lett. 2008;18(15):4388-
841 92.
842 55. Leung AW, Murdoch B, Salem AF, Prasad MS, Gomez GA, Garcia-Castro MI. WNT/beta-
843 catenin signaling mediates human neural crest induction via a pre-neural border intermediate.
844 Development. 2016;143(3):398-410.
845 56. Basch ML, Bronner-Fraser M, Garcia-Castro MI. Specification of the neural crest occurs
846 during gastrulation and requires Pax7. Nature. 2006;441(7090):218-22.
847 57. Simoes-Costa M, Bronner ME. Reprogramming of avian neural crest axial identity and cell
848 fate. Science. 2016;352(6293):1570-3.
849 58. Lumb R, Buckberry S, Secker G, Lawrence D, Schwarz Q. Transcriptome profiling reveals
850 expression signatures of cranial neural crest cells arising from different axial levels. BMC Dev Biol.
851 2017;17(1):5.
852 59. Seo S, Kume T. Forkhead transcription factors, Foxc1 and Foxc2, are required for the
853 morphogenesis of the cardiac outflow tract. Dev Biol. 2006;296(2):421-36.
854 60. Tallquist MD, Soriano P. Cell autonomous requirement for PDGFRalpha in populations of
855 cranial and cardiac neural crest cells. Development. 2003;130(3):507-18.
856 61. Mesbah K, Rana MS, Francou A, van Duijvenboden K, Papaioannou VE, Moorman AF, et al.
857 Identification of a Tbx1/Tbx2/Tbx3 genetic pathway governing pharyngeal and arterial pole
858 morphogenesis. Hum Mol Genet. 2012;21(6):1217-29.
859 62. Young HM, Ciampoli D, Hsuan J, Canty AJ. Expression of Ret-, p75(NTR)-, Phox2a-, Phox2b-,
860 and tyrosine hydroxylase-immunoreactivity by undifferentiated neural crest-derived cells and
861 different classes of enteric neurons in the embryonic mouse gut. Dev Dyn. 1999;216(2):137-52.
862 63. Torihashi S, Yoshida H, Nishikawa S, Kunisada T, Sanders KM. Enteric neurons express Steel
863 factor-lacZ transgene in the murine gastrointestinal tract. Brain Res. 1996;738(2):323-8.
864 64. Iwashita T, Kruger GM, Pardal R, Kiel MJ, Morrison SJ. Hirschsprung disease is linked to
865 defects in neural crest stem cell function. Science. 2003;301(5635):972-6.
866 65. Wildner H, Gierl MS, Strehle M, Pla P, Birchmeier C. Insm1 (IA-1) is a crucial component of
867 the transcriptional network that controls differentiation of the sympatho-adrenal lineage.
868 Development. 2008;135(3):473-81.
869 66. Huber K, Narasimhan P, Shtukmaster S, Pfeifer D, Evans SM, Sun Y. The LIM-Homeodomain
870 transcription factor Islet-1 is required for the development of sympathetic neurons and adrenal
871 chromaffin cells. Dev Biol. 2013;380(2):286-98.
872 67. Perez SE, Rebelo S, Anderson DJ. Early specification of sensory neuron fate revealed by
873 expression and function of neurogenins in the chick embryo. Development. 1999;126(8):1715-28.
874 68. Katoh M, Katoh M. Characterization of human ARHGAP10 gene in silico. Int J Oncol.
875 2004;25(4):1201-6.
876 69. Bainbridge MN, Hu H, Muzny DM, Musante L, Lupski JR, Graham BH, et al. De novo
877 truncating mutations in ASXL3 are associated with a novel clinical phenotype with similarities to
878 Bohring-Opitz syndrome. Genome Med. 2013;5(2):11.
879 70. Heglind M, Cederberg A, Aquino J, Lucas G, Ernfors P, Enerback S. Lack of the central nervous
880 system- and neural crest-expressed forkhead gene Foxs1 affects motor function and body weight.
881 Mol Cell Biol. 2005;25(13):5616-25.
882 71. Rada-Iglesias A, Bajpai R, Prescott S, Brugmann SA, Swigut T, Wysocka J. Epigenomic
883 annotation of enhancers predicts transcriptional regulators of human neural crest. Cell Stem Cell.
884 2012;11(5):633-48.
885 72. Dupe V, Ghyselinck NB, Wendling O, Chambon P, Mark M. Key roles of retinoic acid
886 receptors alpha and beta in the patterning of the caudal hindbrain, pharyngeal arches and otocyst in
887 the mouse. Development. 1999;126(22):5051-9.

888 73. Gibbs BC, Damerla RR, Vladar EK, Chatterjee B, Wan Y, Liu X, et al. Prickle1 mutation causes
889 planar cell polarity and directional cell migration defects associated with cardiac outflow tract
890 anomalies and other structural birth defects. Biol Open. 2016;5(3):323-35.
891 74. Schneider C, Wicht H, Enderich J, Wegner M, Rohrer H. Bone morphogenetic proteins are
892 required in vivo for the generation of sympathetic neurons. Neuron. 1999;24(4):861-70.
893 75. Morikawa Y, Maska E, Brody H, Cserjesi P. Sonic hedgehog signaling is required for
894 sympathetic nervous system development. Neuroreport. 2009;20(7):684-8.
895 76. Pattyn A, Goridis C, Brunet JF. Specification of the central noradrenergic phenotype by the
896 homeobox gene Phox2b. Mol Cell Neurosci. 2000;15(3):235-43.
897 77. Hirsch MR, Tiveron MC, Guillemot F, Brunet JF, Goridis C. Control of noradrenergic
898 differentiation and Phox2a expression by MASH1 in the central and peripheral nervous system.
899 Development. 1998;125(4):599-608.
900 78. Tsarovina K, Reiff T, Stubbusch J, Kurek D, Grosveld FG, Parlato R, et al. The Gata3
901 transcription factor is required for the survival of embryonic and adult sympathetic neurons. J
902 Neurosci. 2010;30(32):10833-43.
903 79. Ernsberger U, Reissmann E, Mason I, Rohrer H. The expression of dopamine beta-
904 hydroxylase, tyrosine hydroxylase, and Phox2 transcription factors in sympathetic neurons: evidence
905 for common regulation during noradrenergic induction and diverging regulation later in
906 development. Mech Dev. 2000;92(2):169-77.
907 80. Troy CM, Brown K, Greene LA, Shelanski ML. Ontogeny of the neuronal intermediate
908 filament protein, peripherin, in the mouse embryo. Neuroscience. 1990;36(1):217-37.
909 81. Delfino-Machin M, Lunn JS, Breitkreuz DN, Akai J, Storey KG. Specification and maintenance
910 of the spinal cord stem zone. Development. 2005;132(19):4273-83.
911 82. Bang AG, Papalopulu N, Kintner C, Goulding MD. Expression of Pax-3 is initiated in the early
912 neural plate by posteriorizing signals produced by the organizer and by posterior non-axial
913 mesoderm. Development. 1997;124(10):2075-85.
914 83. LaBonne C, Bronner-Fraser M. Neural crest induction in Xenopus: evidence for a two-signal
915 model. Development. 1998;125(13):2403-14.
916 84. Funa NS, Schachter KA, Lerdrup M, Ekberg J, Hess K, Dietrich N, et al. beta-Catenin Regulates
917 Primitive Streak Induction through Collaborative Interactions with SMAD2/SMAD3 and OCT4. Cell
918 Stem Cell. 2015;16(6):639-52.
919 85. Desmarais JA, Unger C, Damjanov I, Meuth M, Andrews P. Apoptosis and failure of
920 checkpoint kinase 1 activation in human induced pluripotent stem cells under replication stress.
921 Stem Cell Res Ther. 2016;7:17.
922 86. Rostovskaya M, Fu J, Obst M, Baer I, Weidlich S, Wang H, et al. Transposon-mediated BAC
923 transgenesis in human ES cells. Nucleic Acids Res. 2012;40(19):e150.
924 87. Kim D, Pertea G, Trapnell C, Pimentel H, Kelley R, Salzberg SL. TopHat2: accurate alignment
925 of transcriptomes in the presence of insertions, deletions and gene fusions. Genome Biol.
926 2013;14(4):R36.
927 88. Anders S, Pyl PT, Huber W. HTSeq--a Python framework to work with high-throughput
928 sequencing data. Bioinformatics. 2015;31(2):166-9.
929 89. Love MI, Huber W, Anders S. Moderated estimation of fold change and dispersion for RNA-
930 seq data with DESeq2. Genome Biol. 2014;15(12):550.
931 90. Huang da W, Sherman BT, Lempicki RA. Bioinformatics enrichment tools: paths toward the
932 comprehensive functional analysis of large gene lists. Nucleic Acids Res. 2009;37(1):1-13.
933 91. Huang da W, Sherman BT, Lempicki RA. Systematic and integrative analysis of large gene lists
934 using DAVID bioinformatics resources. Nat Protoc. 2009;4(1):44-57.
935 92. Chen J, Bardes EE, Aronow BJ, Jegga AG. ToppGene Suite for gene list enrichment analysis
936 and candidate gene prioritization. Nucleic Acids Res. 2009;37(Web Server issue):W305-11.
937 93. Micallef L, Rodgers P. eulerAPE: drawing area-proportional 3-Venn diagrams using ellipses.
938 PLoS One. 2014;9(7):e101717.

939 94. Osorno R, Tsakiridis A, Wong F, Cambray N, Economou C, Wilkie R, et al. The developmental
940 dismantling of pluripotency is reversed by ectopic Oct4 expression. Development.
941 2012;139(13):2288-98.

Fig.1

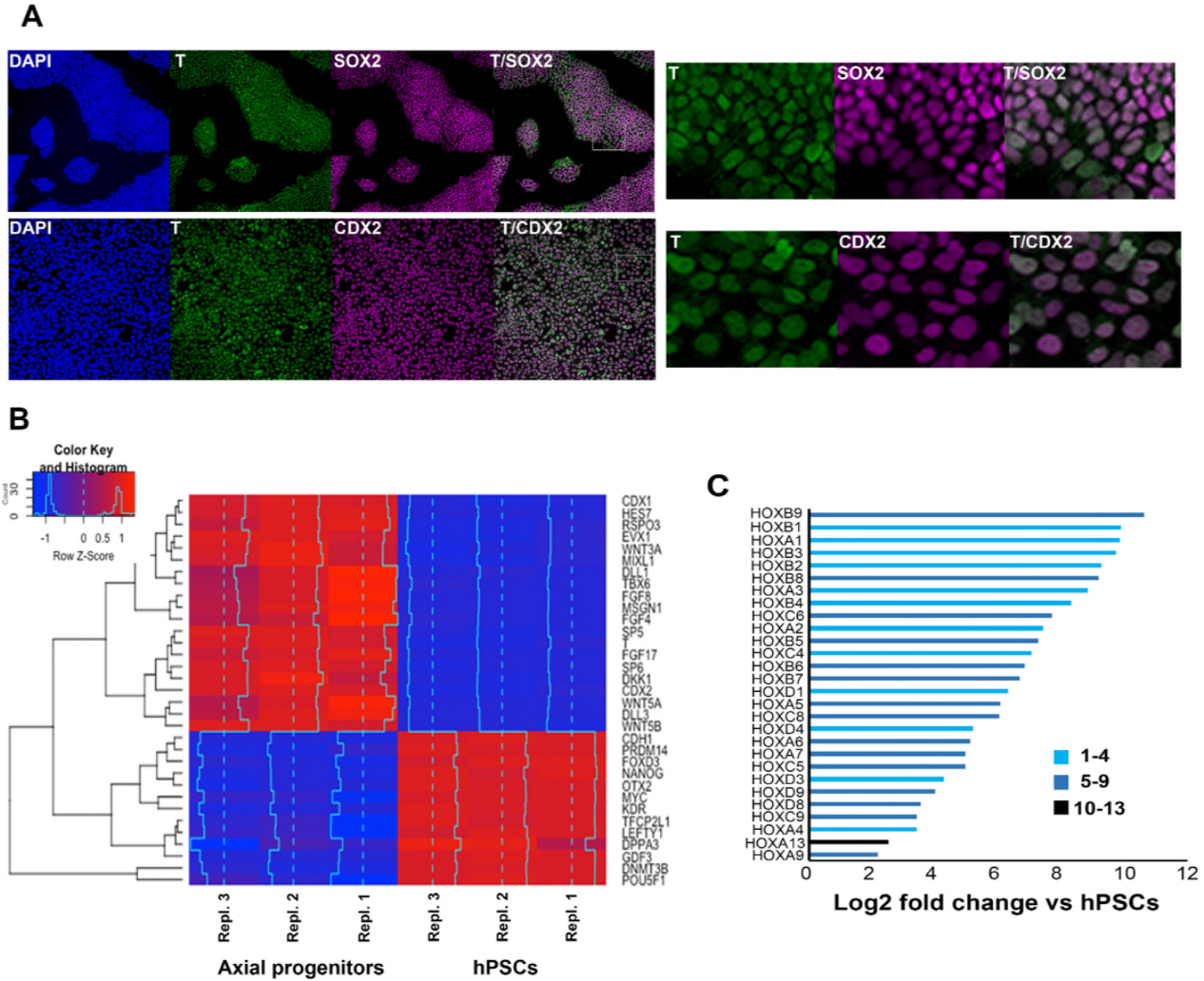
A
DAPI
T
SOX2
T/SOX2
DAPI
T
CDX2
T/CDX2
T
SOX2
T/SOX2
T
CDX2
T/CDX2
B
Color Key and Histogram
Count
0
30
-1
0
0.5
1
Row Z-Score
CDX1
HES7
RSPO3
EVX1
WNT3A
MIXL1
DLL1
TBX6
FGF8
MSGN1
FGF4
SP5
T
FGF17
SP6
DKK1
CDX2
WNT5A
DLL3
WNT5B
CDH1
PRDM14
FOXD3
NANOG
OTX2
MYC
KDR
TFCP2L1
LEFTY1
DPPA3
GDF3
DNMT3B
POU5F1
Repl. 3
Repl. 2
Repl. 1
Repl. 3
Repl. 2
Repl. 1
Axial progenitors
hPSCs
C
HOXB9
HOXB1
HOXA1
HOXB3
HOXB2
HOXB8
HOXA3
HOXB4
HOXC6
HOXA2
HOXB5
HOXC4
HOXB6
HOXB7
HOXD1
HOXA5
HOXC8
HOXD4
HOXA6
HOXA7
HOXC5
HOXD3
HOXD9
HOXD8
HOXC9
HOXA4
HOXA13
HOXA9
1-4
5-9
10-13
0
2
4
6
8
10
12
Log2 fold change vs hPSCs

Fig. 2

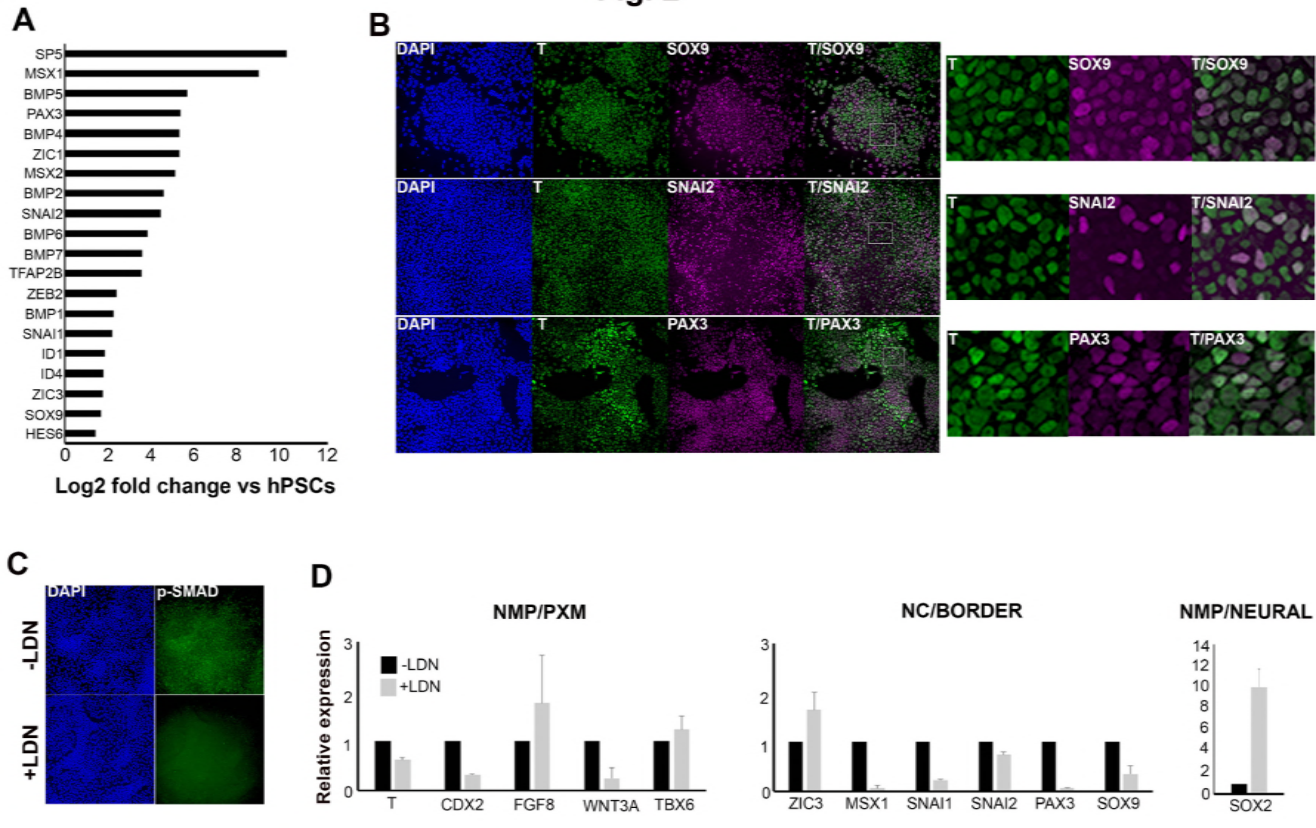
A
SP5
MSX1
BMP5
PAX3
BMP4
ZIC1
MSX2
BMP2
SNAI2
BMP6
BMP7
TFAP2B
ZEB2
BMP1
SNAI1
ID1
ID4
ZIC3
SOX9
HES6
0 2 4 6 8 10 12
Log2 fold change vs hPSCs
B
DAPI
T
SOX9
T/SOX9
DAPI
T
SNAI2
T/SNAI2
DAPI
T
PAX3
T/PAX3
T
SOX9
T/SOX9
T
SNAI2
T/SNAI2
T
PAX3
T/PAX3
C
DAPI
p-SMAD
-LDN
+LDN
D
NMP/PXM
Relative expression
-LDN
+LDN
T
CDX2
FGF8
WNT3A
TBX6
NC/BORDER
ZIC3
MSX1
SNAI1
SNAI2
PAX3
SOX9
NMP/NEURAL
SOX2

Fig. 3

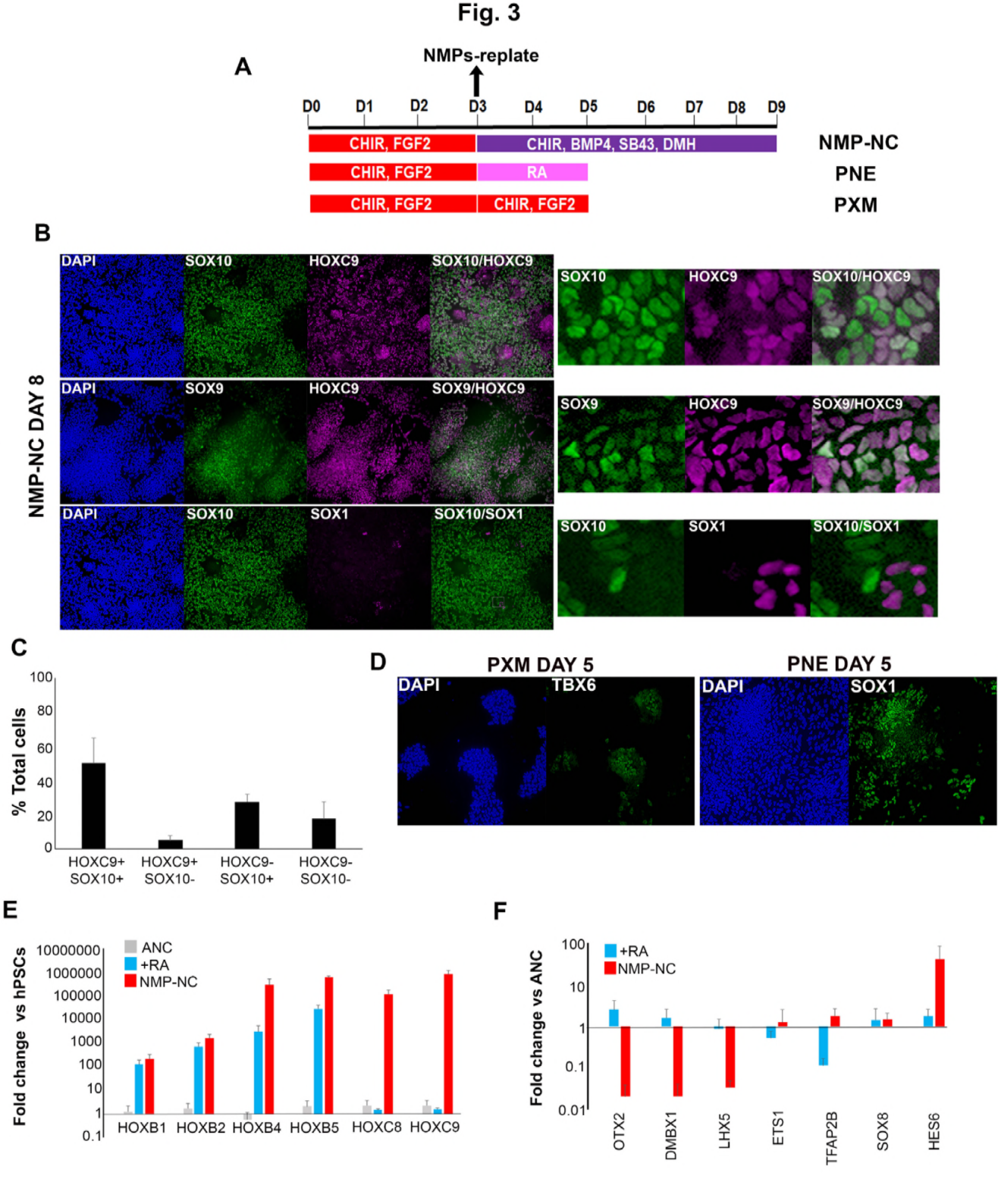
A
NMPs-replate
D0
D1
D2
D3
D4
D5
D6
D7
D8
D9
CHIR, FGF2
CHIR, BMP4, SB43, DMH
NMP-NC
CHIR, FGF2
RA
PNE
CHIR, FGF2
CHIR, FGF2
PXM
B
NMP-NC DAY 8
DAPI
SOX10
HOXC9
SOX10/HOXC9
SOX9
SOX9/HOXC9
SOX1
SOX10/SOX1
C
% Total cells
100
80
60
40
20
0
HOXC9+ SOX10+
HOXC9+ SOX10-
HOXC9- SOX10+
HOXC9- SOX10-
D
PXM DAY 5
PNE DAY 5
DAPI
TBX6
SOX1
E
Fold change vs hPSCs
10000000
1000000
100000
10000
1000
100
10
1
0.1
ANC
+RA
NMP-NC
HOXB1
HOXB2
HOXB4
HOXB5
HOXC8
HOXC9
F
Fold change vs ANC
100
10
1
0.1
0.01
+RA
NMP-NC
OTX2
DMBX1
LHX5
ETS1
TFAP2B
SOX8
HES6

Fig. 4

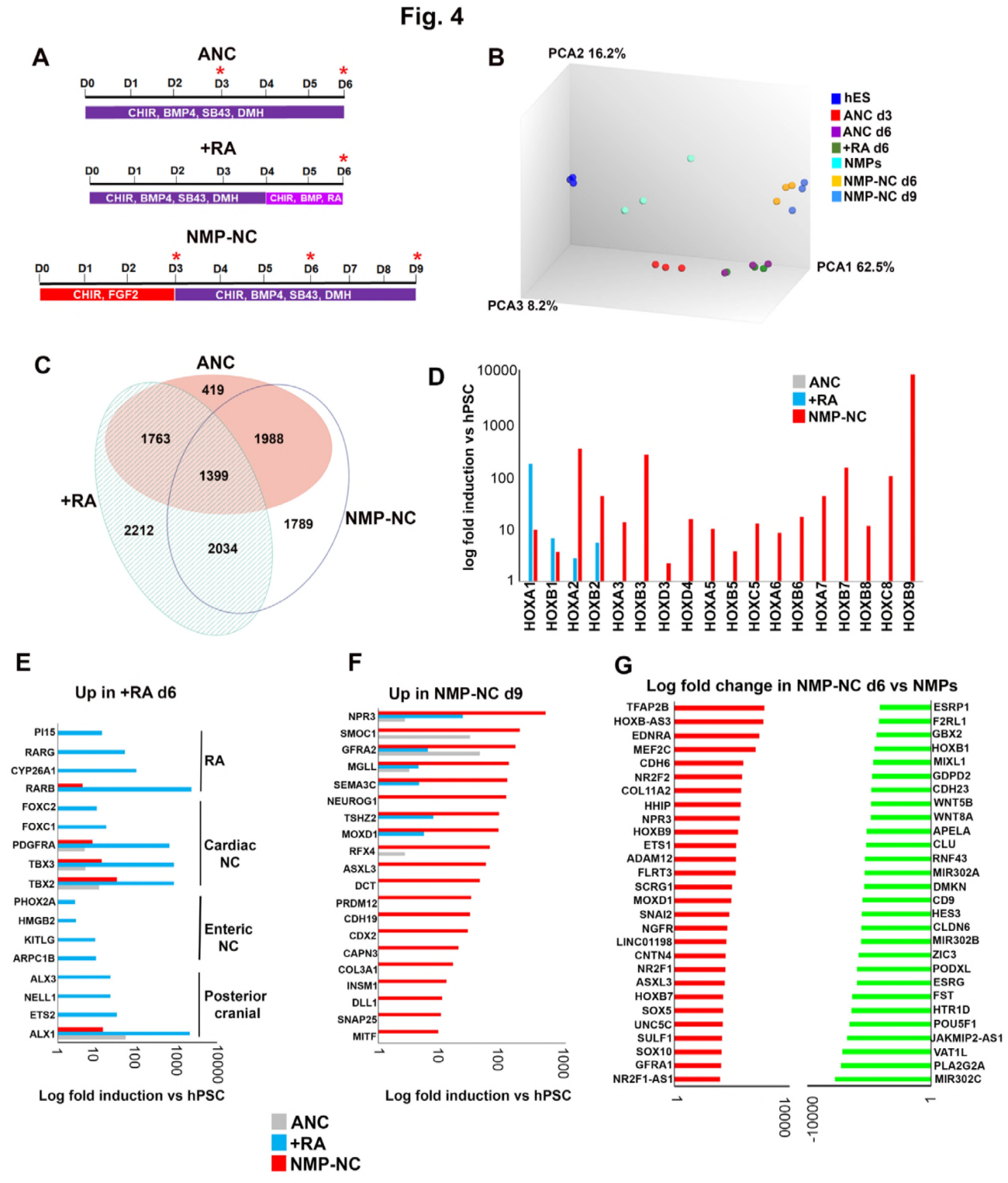
A
ANC
D0 D1 D2 D3 D4 D5 D6
CHIR, BMP4, SB43, DMH
+RA
D0 D1 D2 D3 D4 D5 D6
CHIR, BMP4, SB43, DMH
CHIR, BMP, RA
NMP-NC
D0 D1 D2 D3 D4 D5 D6 D7 D8 D9
CHIR, FGF2
CHIR, BMP4, SB43, DMH
B
PCA2 16.2%
PCA1 62.5%
PCA3 8.2%
hES
ANC d3
ANC d6
+RA d6
NMPs
NMP-NC d6
NMP-NC d9
C
ANC
+RA
NMP-NC
419
1763
1988
1399
2212
1789
2034
D
log fold induction vs hPSC
10000
1000
100
10
1
ANC
+RA
NMP-NC
HOXA1 HOXB1 HOXA2 HOXB2 HOXA3 HOXB3 HOXD3 HOXD4 HOXA5 HOXB5 HOXC5 HOXA6 HOXB6 HOXA7 HOXB7 HOXB8 HOXC8 HOXB9
E
Up in +RA d6
PI15
RARG
CYP26A1
RARB
FOXC2
FOXC1
PDGFRA
TBX3
TBX2
PHOX2A
HMGB2
KITLG
ARPC1B
ALX3
NELL1
ETS2
ALX1
RA
Cardiac NC
Enteric NC
Posterior cranial
1 10 100 1000 10000
Log fold induction vs hPSC
F
Up in NMP-NC d9
NPR3
SMOC1
GFRA2
MGLL
SEMA3C
NEUROG1
TSHZ2
MOXD1
RFX4
ASXL3
DCT
PRDM12
CDH19
CDX2
CAPN3
COL3A1
INSM1
DLL1
SNAP25
MITF
1 10 100 1000
Log fold induction vs hPSC
G
Log fold change in NMP-NC d6 vs NMPs
TFAP2B
HOXB-AS3
EDNRA
MEF2C
CDH6
NR2F2
COL11A2
HHIP
NPR3
HOXB9
ETS1
ADAM12
FLRT3
SCRG1
MOXD1
SNAI2
NGFR
LINC01198
CNTN4
NR2F1
ASXL3
HOXB7
SOX5
UNC5C
SULF1
SOX10
GFRA1
NR2F1-AS1
ESRP1
F2RL1
GBX2
HOXB1
MIXL1
GDPD2
CDH23
WNT5B
WNT8A
APELA
CLU
RNF43
MIR302A
DMKN
CD9
HES3
CLDN6
MIR302B
ZIC3
PODXL
ESRG
FST
HTR1D
POU5F1
JAKMIP2-AS1
VAT1L
PLA2G2A
MIR302C
1 10000
-10000 1
ANC
+RA
NMP-NC

Fig. 5

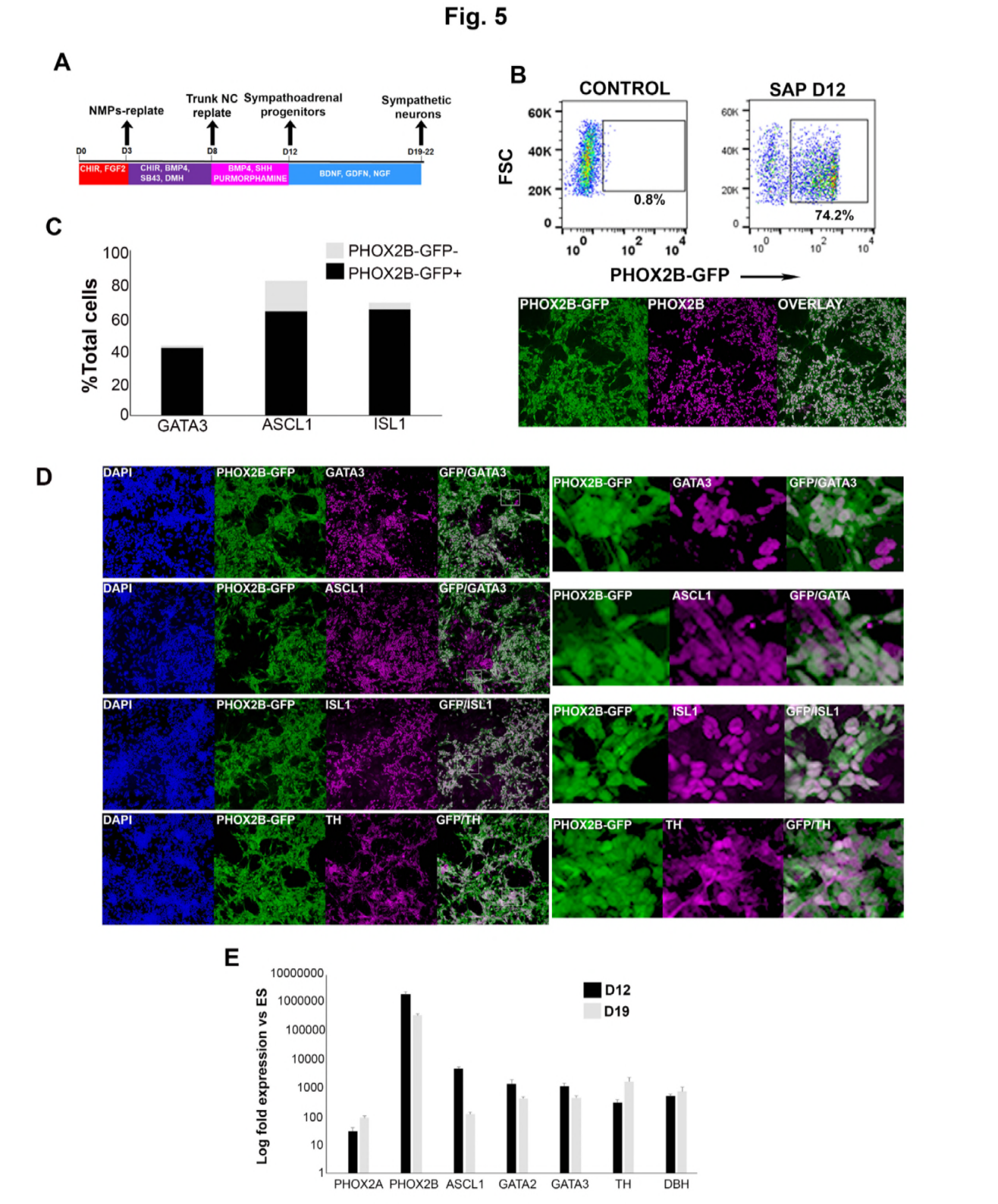
A
NMPs-replate
Trunk NC replate
Sympathoadrenal progenitors
Sympathetic neurons
D0
D3
D8
D12
D19-22
CHIR, FGF2
CHIR, BMP4, SB43, DMH
BMP4, SHH PURMORPHAMINE
BDNF, GDFN, NGF
B
CONTROL
SAP D12
FSC
60K
40K
20K
0
0.8%
74.2%
PHOX2B-GFP
PHOX2B-GFP
PHOX2B
OVERLAY
C
%Total cells
PHOX2B-GFP-
PHOX2B-GFP+
GATA3
ASCL1
ISL1
D
DAPI
PHOX2B-GFP
GATA3
GFP/GATA3
ASCL1
GFP/GATA
ISL1
GFP/ISL1
TH
GFP/TH
E
Log fold expression vs ES
D12
D19
PHOX2A
PHOX2B
ASCL1
GATA2
GATA3
TH
DBH

Fig. 6

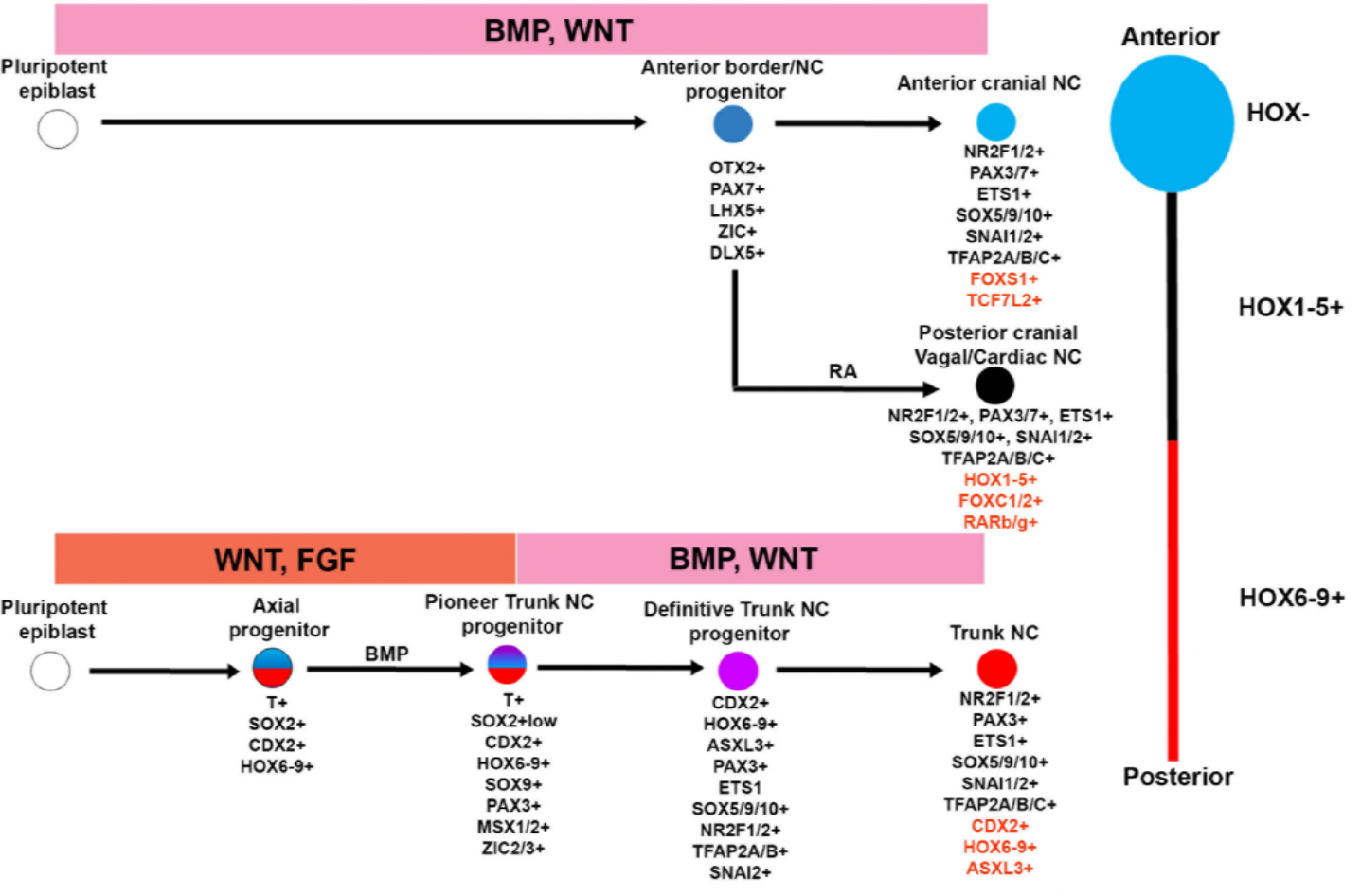
BMP, WNT
Pluripotent epiblast
Anterior border/NC progenitor
Anterior cranial NC
OTX2+
PAX7+
LHX5+
ZIC+
DLX5+
NR2F1/2+
PAX3/7+
ETS1+
SOX5/9/10+
SNAI1/2+
TFAP2A/B/C+
FOXS1+
TCF7L2+
RA
Posterior cranial Vagal/Cardiac NC
NR2F1/2+, PAX3/7+, ETS1+
SOX5/9/10+, SNAI1/2+
TFAP2A/B/C+
HOX1-5+
FOXC1/2+
RARb/g+
Anterior
HOX-
HOX1-5+
HOX6-9+
Posterior
WNT, FGF
BMP, WNT
Pluripotent epiblast
Axial progenitor
BMP
Pioneer Trunk NC progenitor
Definitive Trunk NC progenitor
Trunk NC
T+
SOX2+
CDX2+
HOX6-9+
T+
SOX2+low
CDX2+
HOX6-9+
SOX9+
PAX3+
MSX1/2+
ZIC2/3+
CDX2+
HOX6-9+
ASXL3+
PAX3+
ETS1
SOX5/9/10+
NR2F1/2+
TFAP2A/B+
SNAI2+
NR2F1/2+
PAX3+
ETS1+
SOX5/9/10+
SNAI1/2+
TFAP2A/B/C+
CDX2+
HOX6-9+
ASXL3+

Fig. S1

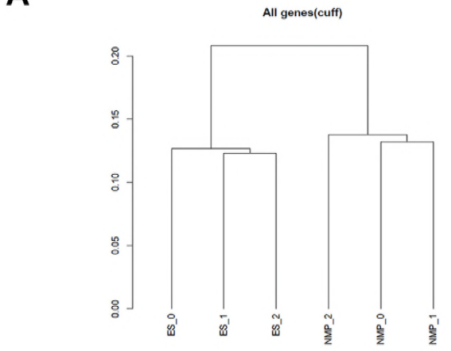
A
All genes(cuff)
0.20
0.15
0.10
0.05
0.00
ES_0
ES_1
ES_2
NMP_2
NMP_0
NMP_1

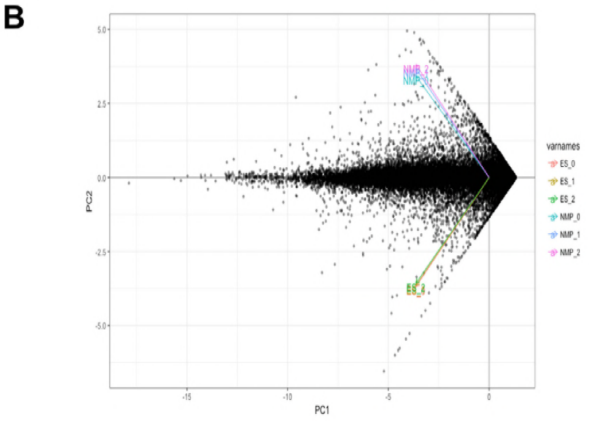
B
PC2
PC1
varnames
ES_0
ES_1
ES_2
NMP_0
NMP_1
NMP_2

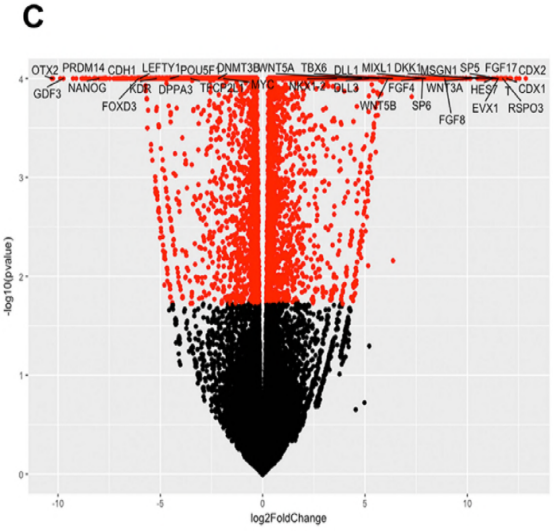
C
OTX2
PRDM14
CDH1
LEFTY1
POU5F1
DNMT3B
WNT5A
TBX6
DLL1
MIXL1
DKK1
MSGN1
SP5
FGF17
CDX2
GDF3
NANOG
KDR
DPPA3
TBCP2L1
MYC
NKX1-2
DLL3
FGF4
WNT3A
HES7
CDX1
FOXD3
WNT5B
SP6
FGF8
EVX1
RSPO3
-log10(pvalue)
log2FoldChange

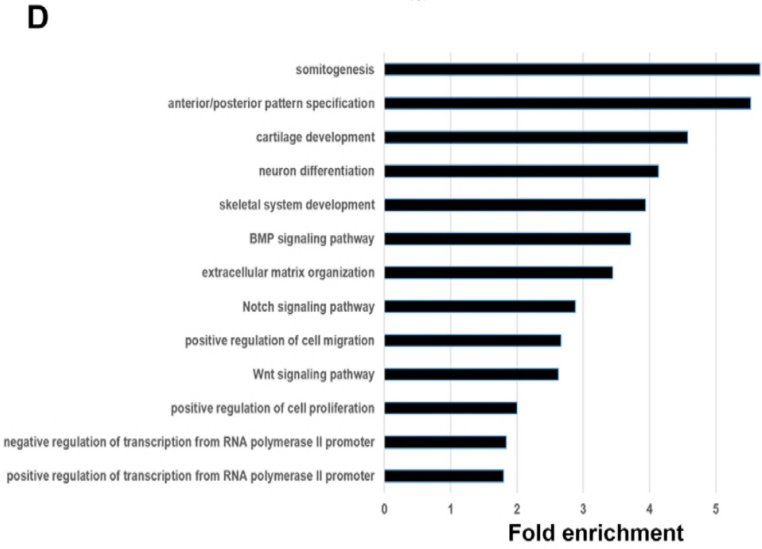
D
somitogenesis
anterior/posterior pattern specification
cartilage development
neuron differentiation
skeletal system development
BMP signaling pathway
extracellular matrix organization
Notch signaling pathway
positive regulation of cell migration
Wnt signaling pathway
positive regulation of cell proliferation
negative regulation of transcription from RNA polymerase II promoter
positive regulation of transcription from RNA polymerase II promoter
Fold enrichment

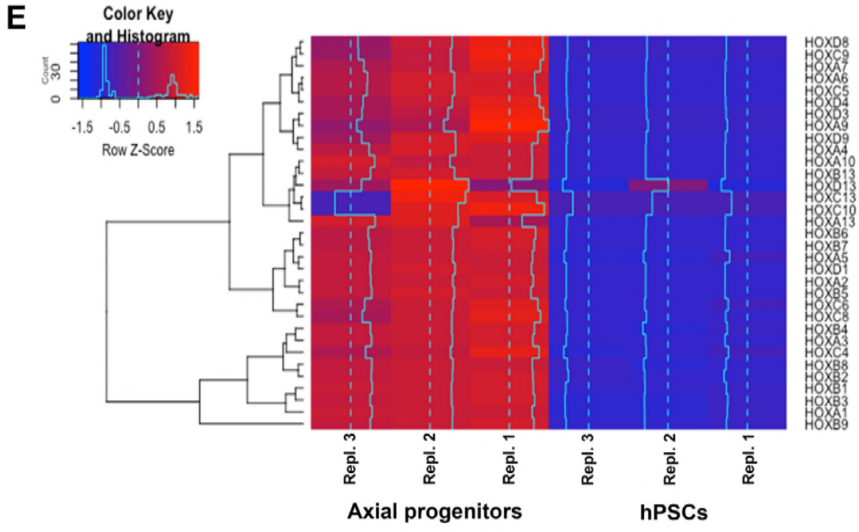
E
Color Key
and Histogram
Count
Row Z-Score
HOXD8
HOXC9
HOXA7
HOXA6
HOXC5
HOXD4
HOXD3
HOXA9
HOXD9
HOXA4
HOXA10
HOXB13
HOXD13
HOXC13
HOXC10
HOXA13
HOXB6
HOXB7
HOXA5
HOXD1
HOXA2
HOXB5
HOXC6
HOXC8
HOXB4
HOXA3
HOXC4
HOXB8
HOXB2
HOXB1
HOXB3
HOXA1
HOXB9
Repl. 3
Repl. 2
Repl. 1
Repl. 3
Repl. 2
Repl. 1
Axial progenitors
hPSCs

Fig. S2

A

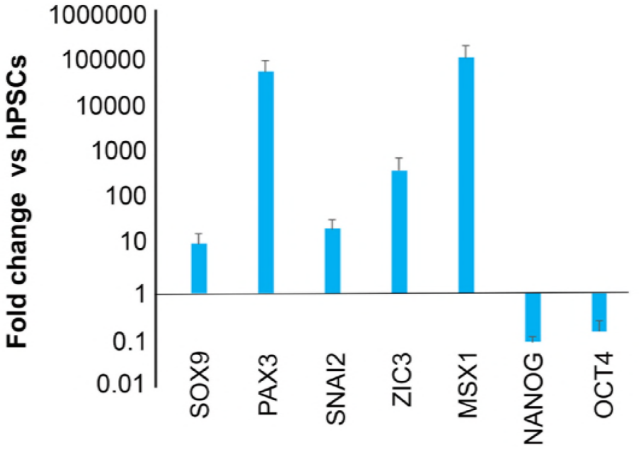
Fold change vs hPSCs
1000000
100000
10000
1000
100
10
1
0.1
0.01
SOX9
PAX3
SNAI2
ZIC3
MSX1
NANOG
OCT4

B

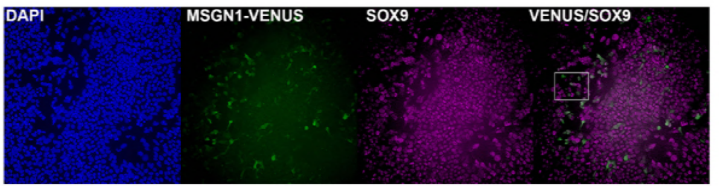
DAPI
MSGN1-VENUS
SOX9
VENUS/SOX9

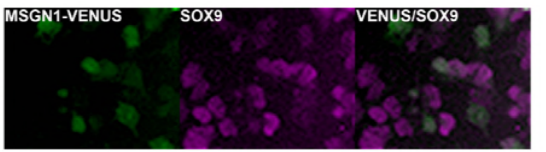
MSGN1-VENUS
SOX9
VENUS/SOX9

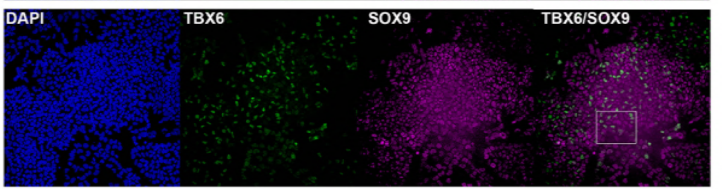
DAPI
TBX6
SOX9
TBX6/SOX9

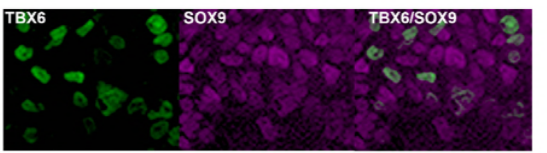
TBX6
SOX9
TBX6/SOX9

Fig. S3

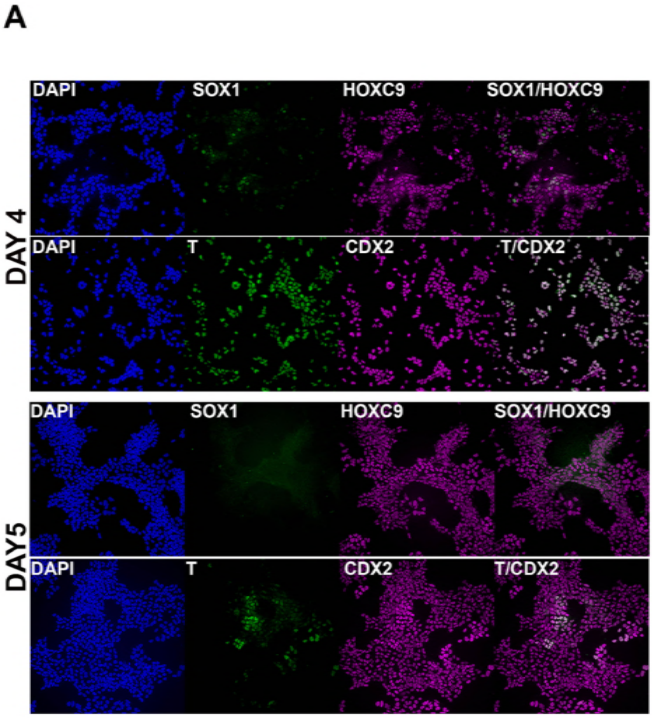
A
DAY 4
DAPI
SOX1
HOXC9
SOX1/HOXC9
DAPI
T
CDX2
T/CDX2
DAY5
DAPI
SOX1
HOXC9
SOX1/HOXC9
DAPI
T
CDX2
T/CDX2

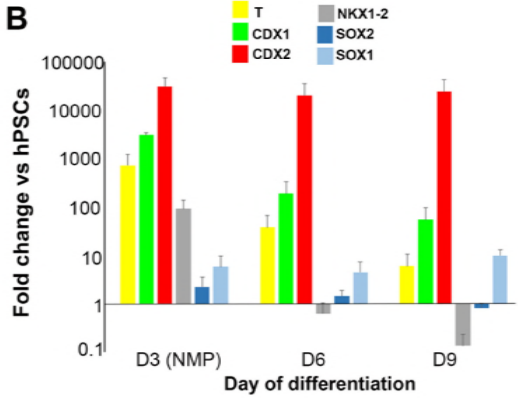
B
T
CDX1
CDX2
NKX1-2
SOX2
SOX1
100000
10000
1000
100
10
1
0.1
Fold change vs hPSCs
D3 (NMP)
D6
D9
Day of differentiation

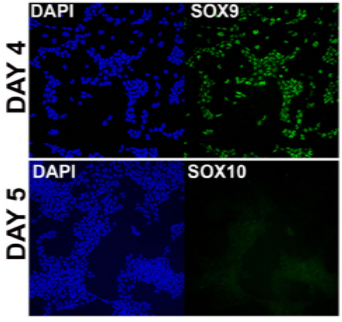
C
DAY 4
DAPI
SOX9
DAY 5
DAPI
SOX10

Fig. S4

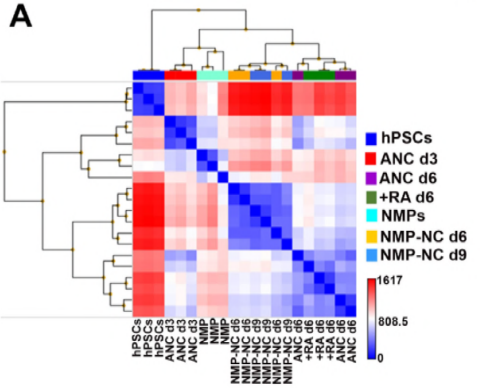
A
hPSCs
ANC d3
ANC d6
+RA d6
NMPs
NMP-NC d6
NMP-NC d9
1617
808.5
0

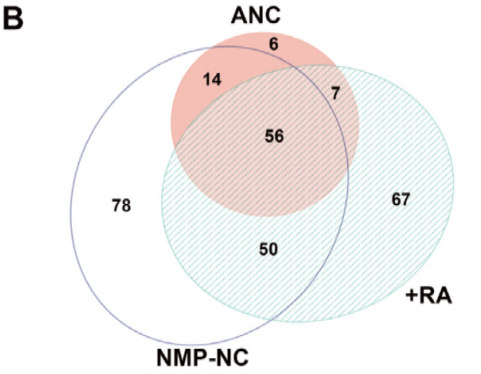
B
ANC
6
14
7
56
78
67
50
+RA
NMP-NC

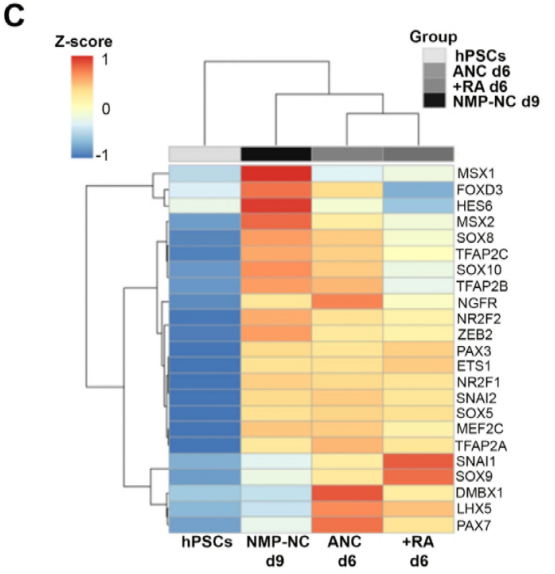
C
Z-score
1
0
-1
Group
hPSCs
ANC d6
+RA d6
NMP-NC d9
MSX1
FOXD3
HES6
MSX2
SOX8
TFAP2C
SOX10
TFAP2B
NGFR
NR2F2
ZEB2
PAX3
ETS1
NR2F1
SNAI2
SOX5
MEF2C
TFAP2A
SNAI1
SOX9
DMBX1
LHX5
PAX7
hPSCs
NMP-NC d9
ANC d6
+RA d6

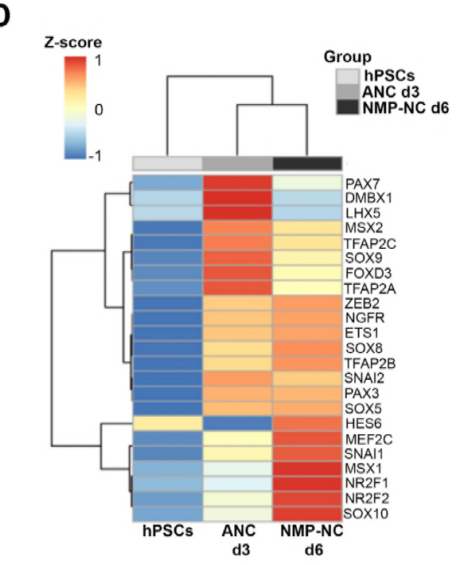
D
Z-score
1
0
-1
Group
hPSCs
ANC d3
NMP-NC d6
PAX7
DMBX1
LHX5
MSX2
TFAP2C
SOX9
FOXD3
TFAP2A
ZEB2
NGFR
ETS1
SOX8
TFAP2B
SNAI2
PAX3
SOX5
HES6
MEF2C
SNAI1
MSX1
NR2F1
NR2F2
SOX10
hPSCs
ANC d3
NMP-NC d6

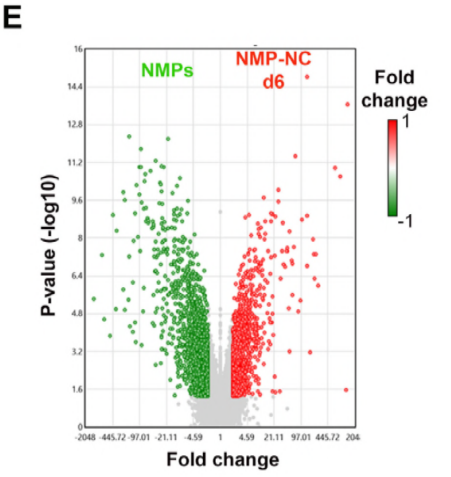
E
NMPs
NMP-NC d6
Fold change
1
-1
P-value (-log10)
Fold change

Fig. S5

A

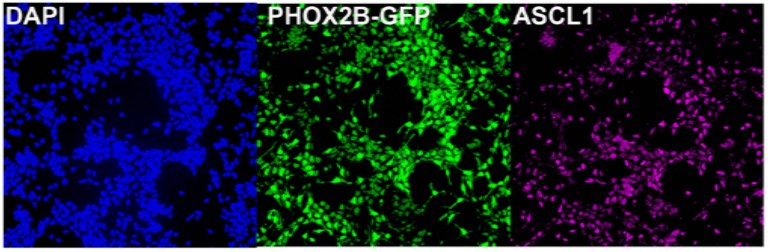

B